RSC Sustainability

ROYAL SOCIETY OF CHEMISTRY

PAPER

View Article Online
View Journal | View Issue



Cite this: *RSC Sustainability*, 2026, **4**, 2729

# Electrified, decentralised upcycling of platinum-group metals from spent automotive catalysts into functional electrocatalysts

Luis F. Leon-Fernandez, †*[a] Frantisek Kukurugya,[a] Omar Martinez-Mora, [ab] Stefanos Mourdikoudis, ‡[a] Lunjie Zeng,[c] Maria M. Parascanu,[d] Aitana Saez,[d] Jan Fransaer, [b] Jeroen Spooren [a] and Xochitl Dominguez-Benetton§*[a]

Securing platinum-group metals (PGMs) for low-carbon technologies requires recycling routes that are both efficient and deployable near the source of waste. We report a fully electrified, modular flowsheet that couples microwave-assisted leaching (MWAL) with gas-diffusion electrocrystallization (GDEx) to recover and upcycle PGMs from spent automotive catalysts. Using 1.5 M HCl + 1.5 M NaCl at up to 200 °C and L/S ≤ 10, MWAL achieves ≥90% PGM leaching while suppressing matrix dissolution at lower L/S. The resulting multielement leachates are treated at room temperature by GDEx (10–200 mA $cm^{-2}$), which selectively converts dissolved PGMs into ~5 nm alloy nanoparticles of ~83–91 wt% purity with >95% metal conversion. The as-recovered nanoparticles act directly as electrocatalysts for the methanol oxidation reaction, delivering MA = 241.7 mA $mg_{Pt}^{-1}$, SA = 0.42 mA $cm^{-2}$, and ~85% activity retention after 1000 cycles. Closed-loop leachate reuse between GDEx and MWAL preserves PGM extraction while progressively reducing matrix co-leaching. Life-cycle assessment identifies MWAL electricity as the primary hotspot (~half of the average impacts), followed by GDEx effluent neutralisation. A 30% heat recovery in MWAL and low-carbon electricity reduces burdens (up to 60% in climate change). A techno-economic assessment at 50 L $h^{-1}$ treatment capacity indicates robust viability (operating margin 13.9%, NPV = 9.08 M€, IRR = 45.1%, 4 year payback), with further gains from scale-up and valorising the nanoparticle product. The MWAL-GDEx route thus offers a scalable, decentralisation-ready, electrified pathway that recovers PGMs with high efficiency and directly upgrades them into functional catalysts.

Received 2nd April 2026
Accepted 14th May 2026

DOI: 10.1039/d6su00190d

rsc.li/rscsus



## Sustainability spotlight

This work advances sustainable chemistry by establishing a fully electrified, low-temperature, modular route to recover platinum-group metals from spent automotive catalysts and directly upcycle them into functional electrocatalysts. By coupling microwave-assisted leaching with gas-diffusion electrocrystallization, the process supports circular use of critical raw materials, reduces reliance on primary mining and centralised smelting, and lowers fresh reagent demand through effluent recirculation. Integrated life-cycle and techno-economic assessment provides evidence-based evaluation of sustainability performance and identifies realistic improvement levers, including heat recovery and low-carbon electricity. This work aligns primarily with UN SDG 12 (Responsible Consumption and Production), and also contributes to SDG 9 (Industry, Innovation and Infrastructure) and SDG 13 (Climate Action).

[a]*Material and Chemistry Unit (MatCh), Flemish Institute for Technological Research (VITO), Boeretang 200, 2400 Mol, Belgium. E-mail: luisfernando_leonfernandez@yahoo.es; xochitldb@gmail.com*

[b]*Department of Materials Engineering, Surface and Interface Engineered Materials, Katholieke Universiteit Leuven, Kasteelpark Arenberg 44 - Box 2450, 3001 Leuven, Belgium*

[c]*Department of Physics, Chalmers University of Technology, 41296 Göteborg, Sweden*

[d]*TECNALIA, Basque Research and Technology Alliance (BRTA), Astondo Bidea, Edificio 700, Derio, 48160, Spain*

† Current affiliation: Applied Electrochemistry & Catalysis (ELCAT), University of Antwerp, Universiteitsplein 1, 2610, Wilrijk, Belgium. E-mail: luisf.leon-fernandez@uantwerpen.be

‡ Current affiliation: CINBIO, Universidade de Vigo, Department of Physical Chemistry, Campus Universitario Lagoas Marcosende, Vigo, 36310 Spain.

§ Current affiliation: Equinor Energy Belgium, Kortenberglaan 120, 1000, Brussels, Belgium. E-mail: luisf.leon-fernandez@uantwerpen.be

## 1. Introduction

The security of supply of critical and strategic metals is now a global policy priority: governments are pivoting from fragile, concentrated primary supply chains towards circularity. Across major economies—including the G7, which launched a Critical Mineral Action Plan—this shift is being underpinned by strategies, legislation, and targets that elevate secondary sourcing.[1] Platinum-group metals (PGMs), including platinum (Pt), palladium (Pd), and rhodium (Rh), are essential catalysts in transportation and industry.[2] Due to their economic significance and potential supply interruption risks, the European Union, United States, United Kingdom, Canada, Australia, Japan, South Korea,

and India classify them as critical raw materials (CRMs).[3–10] PGMs are overwhelmingly imported, with demand dominated by automotive catalysts.[11] With primary supply concentrated in South Africa and Russia—which together account for >80% of global production—accelerating secondary recovery is strategic.[3]

Secondary PGM streams are typically higher-grade and less energy-intensive than primary ores.[11] Yet, only ~35% of global PGM supply was met by recycling in 2024 (mainly from spent automotive catalysts),[12] underscoring the need for more efficient and sustainable recovery technologies.[11] This shortfall reflects a system built around a few centralised pyrometallurgical hubs (*e.g.*, Umicore, Johnson Matthey, Heraeus, and BASF—predominantly located in Western Europe). By contrast, collection and pre-treatment are highly fragmented. End-of-life (EoL) vehicles are transferred from dismantlers to automotive-catalyst aggregators for decanning (removal of the ceramic monolith), milling/crushing, and independent sampling and analysis to produce a homogenised composite, before long-haul shipment to a smelter/refinery. Significant material losses are linked to this value chain structure.

Each hand-off—introduced to satisfy regulatory requirements (*e.g.*, EoL vehicle transport, hazardous waste shipping, permits, chain-of-custody), technical and safety requirements, and settlement needs (verified PGM content for payment, hedging, and metal accounting between seller and refiner)—adds distance, delay, and leakage risk. Additional losses arise from overlooked low-grade PGM sources (*e.g.*, low-loading catalysts, diesel particulate filters, industrial residues) that are uneconomic for central facilities but could be captured by smaller, local units. Moreover, a substantial share of PGM-bearing material never enters the chain at all. Uncollected catalytic converters, unreturned homogeneous catalysts (fine chemicals/pharma), under-recovered material from established sources (petroleum-reforming catalysts, nitric-acid gauzes, glass bushings/equipment, dental alloys, lab sweepings, plating baths/sludges), and heterogeneous catalysts from emerging processes (advanced chemical loops, biomass processing, electrolysers, power-to-X technologies), depress the available recycling feed. There are no harmonised global statistics; as a conservative assumption, the lost recovery opportunity could be on the order of ~10–20% of annual PGM demand (see SI-I for basis and sensitivity).

Shifting to more sustainable, localised processing (*e.g.*, modular, electrified hydrometallurgical systems) can minimise transport costs, simplify supply chains, reduce handling-induced losses, lower environmental impacts, and bring currently overlooked low-grade streams into the spotlight.[13] Provided that (i) local units comply with permitting, safety, and wastewater limits; (ii) selectivity and yields remain acceptable across mixed feeds; (iii) unit economics are viable at the intended scale; (iv) electricity costs are compatible with low-carbon, electrified operation; and (iv) siting near dismantlers reduces logistics burdens, these systems offer a credible pathway to decentralised PGM recovery, substantiated by the evidence presented in the present work.

Conventional PGM recovery, particularly pyrometallurgy, is energy-intensive and emission-heavy.[14] By contrast, hydrometallurgical routes operate at lower temperatures and offer high metal selectivity, reducing environmental impacts.[15] In this context, microwave (MW) heating has emerged as a promising intensification strategy, accelerating reaction kinetics, lowering energy demand, and shortening processing times.[16–19] Coupled with downstream electrochemical recovery, this could enable fully electrified PGM flowsheets.

The EU H2020 PLATIRUS project developed a microwave-assisted leaching (MWAL) process (TRL 5) for PGM extraction from spent automotive catalysts. Extraction efficiencies of 91.8% Pd, 96.0% Pt, and 89.9% Rh were achieved using a single step (10 min) in 6 M HCl with 10 vol% $H_2O_2$, at 150 °C. In the same study it was demonstrated that the *in situ* generation of $Cl_2$ further removed the need for an external oxidising agent (*e.g.*, $H_2O_2$), as high PGM extraction efficiencies were achieved ($93.9 \pm 0.7\%$ for Pd, $98 \pm 3\%$ for Pt, and $70.7 \pm 0.4\%$ for Rh) for a spent automotive catalyst (SAC), using 6 M HCl alone.[20] When applied to unground catalyst monoliths ($\sim 3 \times 3 \times 3$ cm), the process also delivered >95% Pt and Rh recovery using only 6 M HCl, without oxidants.[21] Compared with traditional leaching, MWAL shortens processing time and requires less concentrated acid solutions.[22] Further details on the development and validation of this process can be found in prior PLATIRUS publications.[13,20,21]

The subsequent EU H2020 PEACOC project scaled and optimised MWAL (TRL 7), including lowering HCl concentration below 6 M and partial substitution with NaCl as a low-cost chloride source.[23] These advances support cost-effective and scalable leaching of PGMs under milder, less corrosive conditions. Building on this, the present study validates MWAL at a larger scale and assesses its integration with a suitable downstream PGM recovery and upcycling step—gas-diffusion electrocrystallisation (GDEx).

GDEx, which was also developed in the PLATIRUS project (TRL 5) and upscaled in the PEACOC project (TRL 7), is an emerging electrochemical technology that enables the recovery of metals as (hydr)oxides[24,25] or in the zero-valent metallic form as nanoparticles (NPs).[26–29] The process utilises a gas diffusion electrode (GDE) as the cathode, enabling the percolation and electrochemical reduction of a gas supplied within its porous structure. GDEx can operate through different embodiments depending on the gas, electrolyte composition, and target metal species. In the $CO_2$-fed mode used for PGM recovery, $CO_2$ reduction can generate CO, while hydrogen evolution predominantly arises from proton reduction (in acidic conditions).[26,30]

Previous GDEx studies have shown that these electrogenerated species can contribute to the reduction of PGM chloride complexes (*e.g.*, $[PtCl_6]^{2-}$, $[PdCl_4]^{2-}$, $[RhCl_6]^{3-}$), promoting the formation of metallic nanoparticles. However, their relative contributions depend on the electrolyte composition, applied current density, gas transport, and local interfacial conditions.[26–29] In addition, dissolved $CO_2/HCO_3^-$ provides local buffering, which helps suppress metal hydroxide precipitation and favours controlled nucleation and growth of metallic PGM NPs. The applied current, therefore, affects both

the generation rate of reducing species and the local supersaturation conditions. Additionally, CO may adsorb onto nascent NP surfaces, thereby limiting particle growth and promoting the formation of nanosized metallic particles.[26,27] A schematic overview of the GDEx mechanism for PGM reduction and nanoparticle formation is presented in Fig. S1 (SI-II), along with the corresponding thermodynamic equations (SI-III).

In previous work, using a model solution representative of MWAL leachates, we showed that GDEx could selectively precipitate PGMs from complex aqueous matrices.[26] Here, we validate GDEx with real MWAL-derived leachates and integrate MWAL-GDEx to achieve a fully electrified operation. Applied to PGMs, GDEx operates under mild processing conditions (room temperature and ambient pressure), consuming only $CO_2$ and electricity, making it an attractive and sustainable method.[26,29] Beyond recovery, the resulting PGM NPs enable functional reuse. While conventionally recycled PGMs return mainly to automotive catalysts,[13] the ongoing transition towards electrification and decarbonisation is increasing demand for PGMs in electrolysers and fuel cell technologies.[31] In this context, GDEx-derived PGMs can be directly used as unsupported (electro) catalysts, *e.g.*, for the oxygen reduction reaction (ORR)[32] or the methanol oxidation reaction (MOR).[27,33]

In this work, we establish a fully electrified and circular value chain for the extraction, recovery, and upcycling of PGMs from spent automotive catalysts by coupling MWAL and GDEx. This integrated approach enables selective leaching and recovery of PGMs through nanoparticle formation, entirely powered by electricity, providing a scalable, low-carbon alternative to conventional metallurgical routes. The electrified coupling of MWAL and GDEx demonstrates the feasibility of closing the PGM loop within a decentralised, modular framework that aligns with future net-zero and circular economy targets. Recovered PGMs are directly upcycled as high-performance electrocatalysts for methanol oxidation, showcasing the functional reuse of critical metals. The process is further evaluated through life-cycle assessment (LCA) and a techno-economic analysis (TEA), confirming its potential to deliver sustainable, cost-competitive, and industrially viable PGM recycling.

## 2. Materials and methods

### 2.1. Materials for MWAL

The feedstock sample used in this study, consisting of a mixture of spent three-way automotive catalysts, was provided by MONOLITHOS Catalyst Ltd. (Athens, Greece). It was delivered as a powder with a particle size < 2 mm. The moisture content of the as-delivered sample, determined at 40 °C, was 0.4 wt%. No further pre-treatment was applied prior to MWAL. A detailed explanation of the analytical methods used to characterise the samples is provided in the SI (SI-II, Section 2.1).

As a leaching media, different mixtures of aqueous HCl solutions (fuming, 37% analytical grade, Merck) and NaCl (>99.5% analytical grade, Merck) were employed in various ratios. All solutions were prepared with Milli-Q water.

**2.1.1. MWAL optimisation experiments.** The optimisation of MWAL was performed using a 1 L single-chamber MW reactor (Milestone® SynthWave). The reactor configuration involved mono-mode MW irradiation at 2.45 GHz with a maximum power of 1500 W. In each experiment, 50 g of automotive catalyst sample were utilised, with leaching solution volumes set at 500 mL, 350 mL, or 250 mL, resulting in liquid-to-solid (L/S) ratios of 10, 7, or 5, respectively. The leaching solutions included 1.5 M HCl + 1.5 M NaCl (optimised previously) or 6 M HCl (used as a reference).[23] Mechanical stirring at 50% intensity (295 rpm) was maintained throughout the experiments. The heating time was set to 15 minutes, with a dwell time of 5 minutes, leading to a total MWAL treatment duration of 20 minutes. Temperatures of 150 °C, 180 °C, and 200 °C were tested. Following the dwelling at the selected temperature, the reactor was cooled down for approximately 30 minutes. Monitoring the power used during leaching facilitated the estimation of energy consumption, a parameter essential for LCA calculations.

The downstream operations of MWAL were carried out in a fume hood, including vacuum Büchner filtration with 0.45 μm Whatman filter paper. The filtrates were collected and their volumes quantified. Subsequently, the solid residues were washed over the filter with 250 mL Milli-Q water, and the washing waters were collected and quantified. Leachates and washing water were analysed by ICP-OES after pH and ORP measurements. Solid residues were also analysed by ICP-OES after acid digestion.

### 2.2. Gas-diffusion electrocrystallization (GDEx)

The expanded materials and methods employed for GDEX investigations are presented in the SI (SI-II, Section 2.2). Briefly, the electrochemical reactor consisted of an ElectroCell (EC) Micro Flow Cell, using a three-compartment configuration (Fig. S1a, SI-II, Section 2.2): anolyte, catholyte, and gas chamber in which $CO_2$ (99.99%, Air Liquide) was supplied. In the cathode chamber, a VITO CoRE® activated-carbon-based gas-diffusion electrode (GDE) was used as the cathode, with a projected geometric surface area of 10 $cm^2$. The specifications of VITO CoRE® GDEs can be found in previous works.[34] No electrocatalysts were incorporated into this electrode. A leak-free Ag/AgCl (3 M KCl) reference electrode (eDAQ) was placed near the GDE (~1 mm). The anode was a Pt-coated Ta plate (5 mm thick with a 10 μm thick Pt coating), with a projected geometrical surface area of 10 $cm^2$. A reinforced Zirfon® ion-permeable separator (Pearl UTP 500) was used between the two electrolyte compartments. All current densities mentioned within this work refer to the projected geometric surface area of the GDE. Catholyte and anolyte were pumped to the electrochemical cell from external cathodic and anodic reservoirs, respectively, at a liquid flow rate of 100 mL $min^{-1}$, in an experimental system analogous to the one reported in our previous works on GDEx.[24] In the present research, the electrolyte was recirculated in each corresponding loop (external reservoir-electrolyte compartment in the cell-external reservoir), thus operating in batch mode with recirculation. Magnetic stirring at around 600 rpm was set in the cathodic and anodic external reservoirs outside the electrochemical reactor. Experiments were conducted at room

temperature (approximately 22 °C). The anolyte consisted of a 250 mL 0.5 M NaCl aqueous solution. Conversely, the catholyte consisted of a 100 mL aqueous solution containing the PGM-containing leachate sample from the MWAL unit. Chronopotentiometric (CP) experiments were carried out in batch mode at 10 mA $cm^{-2}$, 40 mA $cm^{-2}$ or 200 mA $cm^{-2}$ using a Biologic VSP3 Potentiostat. The pH, charge and potential were monitored on-line. For most experiments, two replicates were conducted per experiment. The plotted results are replicate averages. The product characterisation techniques and the electrocatalytic activity testing are described in the SI (SI-II, Section 2.2 and 2.3).

### 2.3. Life-cycle assessment (LCA)

The LCA was conducted in accordance with the ISO 14040/14044 (2006) standard, which provides a structured methodology for evaluating the environmental impacts associated with all stages of a product's life cycle. This includes the extraction, processing, and transport of raw materials, as well as emissions, energy use, and waste generation. The LCA followed the standard four-stage approach: goal and scope definition, life cycle inventory (LCI), impact assessment (LCIA), and interpretation.[35]

**2.3.1. Goal and scope.** This analysis screens the environmental performance of a new route for recovering PGMs from automotive catalysts, based on laboratory data. These preliminary findings are expected to help identify potential hotspots of the new technology, thereby providing essential information for optimising the process when further scaled (*e.g.,* to TRL 7).

The functional unit (FU) is 1 g of recovered PGMs.

**2.3.2. System boundaries.** A grave-to-gate boundary was applied for the PGMs MWAL-GDEx route using the EoL automotive catalysts content (LCA grave boundary) as feedstock. This route (Fig. 3a) includes a first stage in which the manual separation of PGM-bearing ceramic monoliths from spent automotive catalysts is performed, followed by size reduction through ball milling. The PGM-bearing powder is directed to the refining stage, which combines the two described technologies. First, the novel hydrometallurgical technology based on MWAL is used for the extraction of PGMs from the automotive catalyst powder. GDEx then processes the resulting PGM-bearing leachate to selectively recover the PGMs into a mixed slurry (LCA gate boundary). Transport between milling and refining stages is not included, as it is not representative of a potential upscaled solution and could lead to misinterpretation.

PGMs resulting from the GDEx process can have different fates. Mixed PGM slurries can be sent for refining in a smelter, which is the baseline case considered in the TEA. This would also be the standard practice when recycling is carried out *via* centralised pyrometallurgical hubs. Otherwise, the GDEx-produced PGM-bearing slurries can be redissolved (*e.g.*, nitric acid) for re-manufacturing of catalytic converters. Although the latter case was validated throughout the PLATIRUS project,[13] it is not the highest value strategy. When using the conditions described in the present paper, the product of GDEx is a mix of PGM NPs (slurry)—a high-value product. Due to the gate boundary imposed for the LCA, the use-phase and end-of-life phase (aka fate) of the mixed PGM slurry is irrelevant (cut-off model), and system expansion is not used to estimate avoided impacts. The estimation of avoided impacts—such as those resulting from substituting primary extraction of PGMs with recovery from waste is considered out of scope for the present assessment. This is different for the TEA, where fate determines profitability. Thus, the TEA compares the lowest and highest fate scenarios: (i) baseline recycling (slurry sent to a smelter/refinery), and (ii) functional upcycling (slurry used as PGM nanoparticles for direct applications).

**2.3.4. Life cycle inventory assessment (LCI).** The foreground (primary) data was collected at the laboratory scale with a current density of 200 mA $cm^{-2}$ and NaCl conditions for GDEx and L/S of 5 for MWAL. This latter L/S ratio was found, in the experimental work, to offer improved selectivity, reduced mass loss, and lower energy demand in the MWAL stage, as well as high recovery rates and decreased energy demand in GDEx; therefore, a sensitivity analysis of this parameter was deemed unnecessary. The background data, encompassing energy and consumables production, as well as emissions and waste treatment, were obtained from specific LCA databases (Ecoinvent v3.11). The data used are representative of Europe.

The LCI for the recovery of 1 g of PGMs from the automotive catalyst is summarised in Table S2 (SI-II, Section 2.4). SimaPro 9.5 was used to model the process and calculate potential environmental impacts.

**2.3.5. Life cycle impact assessment (LCIA).** The selection of impact categories was based on a materiality analysis that combined evidence from scientific literature with expert input from the PEACOC project consortium. The impact categories identified as significant are: Climate Change (CC), ozone layer depletion (OD), photochemical ozone formation (POF), particulate matter formation (PMF), human toxicity—cancer (HTc), human toxicity—non-cancer(HTnc), acidification (AC), eutrophication (EP), freshwater ecotoxicity (ETX), water footprint (WF), abiotic resource depletion of elements (ADe), abiotic resource depletion fossil fuels (ADff), and cumulative energy demand (CED).

**2.3.6. Assumptions and limitations.** The LCA results presented in this study are based on laboratory-scale data, which introduces inherent limitations when extrapolating to industrial-scale performance. In particular, reagent and energy consumption at lab scale are typically not optimised and may not reflect industrial efficiencies, where process integration is expected to reduce environmental burdens. Conversely, potential losses in recovery yields and additional process steps (such as logistics) at larger scale may increase impacts per functional unit. Therefore, the results should be interpreted as a preliminary or screening-level LCA and future work will include scenario analysis at industrial scale. The LCA model already incorporates selected scale-up assumptions, including a 30% recovery of process heat and the recirculation of effluent streams (from GDEx to MWAL and within MWAL, Fig. 5). These measures aim to better approximate expected industrial conditions and partially account for process integration

strategies that will be implemented at a larger scale. Transportation between stages (MWAL-GDEx) was not included; although inter-stage transport did take place in the present experimental research, it is not representative of scaled up practice, where these stages will be integrated within a single facility, avoiding intermediate transport. For the GDEx effluent treatment, only NaOH dosing for neutralisation and precipitation of dissolved metal ions was considered, based on the measured effluent composition and the product solubility products ($K_{sp}$) of the corresponding metal hydroxides. The resulting precipitate was represented as inert waste as a proxy. This simplified approach does not account for potential co-precipitation phenomena, incomplete separation or the presence of complexing agents that may affect removal efficiency. In addition, downstream treatment steps (*e.g.*, solid–liquid separation, sludge conditioning or potential recovery of valuable metals from the precipitate) were not included. As a result, the environmental impacts associated with effluent management may not be accurate and should be refined in future work using more detailed process data. The European average electricity mix from Ecoinvent v3.11 was used for all three stages (milling, MWAL, and GDEx).

### 2.4. Techno-economic assessment

A TEA was conducted to evaluate the financial viability of the integrated MWAL-GDEx process for recovering PGMs from spent automotive catalysts. This assessment focused on key financial metrics, including the net present value (NPV), which was calculated to determine the profitability of the process by measuring the difference between the present value of cash inflows and outflows over the project's lifetime. The discount rate, $r$, is used in the NPV calculation to convert future (after-tax, pre-financing) project cash flows to present value. The discount rate is typically assumed to be equal to the weighted average cost of capital (WACC) under standard financial conditions. The WACC reflects the average rate of return required by all investors to finance the company's assets and serves as a critical threshold for investment decisions. A project yielding a positive NPV, particularly when calculated with a discount rate equal to the WACC, indicates its ability to generate returns exceeding its capital costs, thus showcasing its economic viability. The WACC was calculated according to standard financial formulas, ensuring an accurate reflection of the cost of equity and debt involved in the project. Accumulated cash flows were also determined, involving the projection of net cash inflows and outflows over time, discounting them to present value, and summing them to evaluate overall financial performance over the project duration. Additionally, the operating profit margin (also known as Earnings Before Interest and Taxes, EBIT) was assessed to evaluate the efficiency of the process in converting revenue into profit after covering operating expenses. The return on investment (ROI) was calculated to measure the profitability relative to the cost of investment. The complete TEA methodology including the formulas for WACC, NPV, EBIT, and ROI determination are provided in the SI (SI-II, Section 2.5).

## 3. Results

### 3.1. Characterisation of the initial sample

XRD analysis identified the main crystalline phases in the spent automotive catalyst powder as cordierite ($Mg_2Al_4Si_5O_{18}$), tazheranite ($(Zr,Ti,Ca)O_2$), cerianite ($CeO_2$), and corundum ($Al_2O_3$). The PGM content, determined by ICP-OES after acid digestion, was 1700 mg per kg Pd, 943 mg per kg Pt, and 272 mg per kg Rh based on the monolith-powder composition. The full elemental composition is presented in Table S3 (SI-IV, Section 4.1). Particle size distribution (Fig. S3, SI-IV, Section 4.1) indicates that more than 50 wt% of the sample consists of particles with sizes <0.5 mm.

### 3.2. Microwave-assisted leaching (MWAL) optimisation

Fig. 1a, presents the extraction efficiencies of PGMs using MWAL in the two leaching systems at three temperatures. A clear positive correlation is observed between leaching temperature and the extraction efficiencies of Pt and Rh in both leaching systems. At 200 °C, the highest efficiencies were obtained: 95 ± 1% Pd, 102 ± 7% Pt, and 107 ± 18% Rh with 6 M HCl, and 90 ± 1% Pd, 96 ± 1% Pt, and 93 ± 18% Rh with 1.5 M HCl + 1.5 M NaCl. These results are consistent with previous reports.[21] Extraction efficiencies exceeding 100% are most likely due to a combination of sample heterogeneity and analytical uncertainties. Material heterogeneity can lead to differences in metal distribution between the aliquots used for initial characterisation and leaching experiments. In addition, ICP-OES signals may be slightly affected by matrix effects (6 M HCl *vs.* 1.5 M HCl + 1.5 M NaCl). The relatively large error bars observed for Rh reflect its low concentration in the sample, where small absolute deviations translate into pronounced relative variability between initial sample and leachates analyses. Therefore, values exceeding 100% should be interpreted as near-complete extraction within experimental uncertainty.

Although PGM extraction was slightly lower with the diluted HCl + NaCl system (see Tables S4 and S5; SI-IV, Section 4.1), this leaching medium demonstrated superior selectivity toward PGMs, significantly reducing the co-extraction of matrix elements such as Al, Ce, and Mg. As shown in Fig. 1b, the enhanced selectivity resulted in nearly 50% lower mass loss compared to the 6 M HCl system.

From an industrial perspective, the liquid-to-solid (L/S) ratio is a crucial parameter that influences throughput and downstream processing. As shown in Fig. 1c, reducing the L/S ratio from 10 to 5 caused only a marginal decrease in PGM extraction efficiency, while generating a more concentrated leachate (detailed composition in Table S6; SI-IV, Section 4.1). Fig. 1d confirms improved selectivity at lower L/S, and Fig. 1e highlights the corresponding decrease in mass loss and energy demand. The latter is attributed to the reduced solution volume per unit mass of catalyst, decreasing the energy required to heat the leaching medium. These findings underscore the potential for resource and energy efficiency gains through optimisation of the L/S ratio.

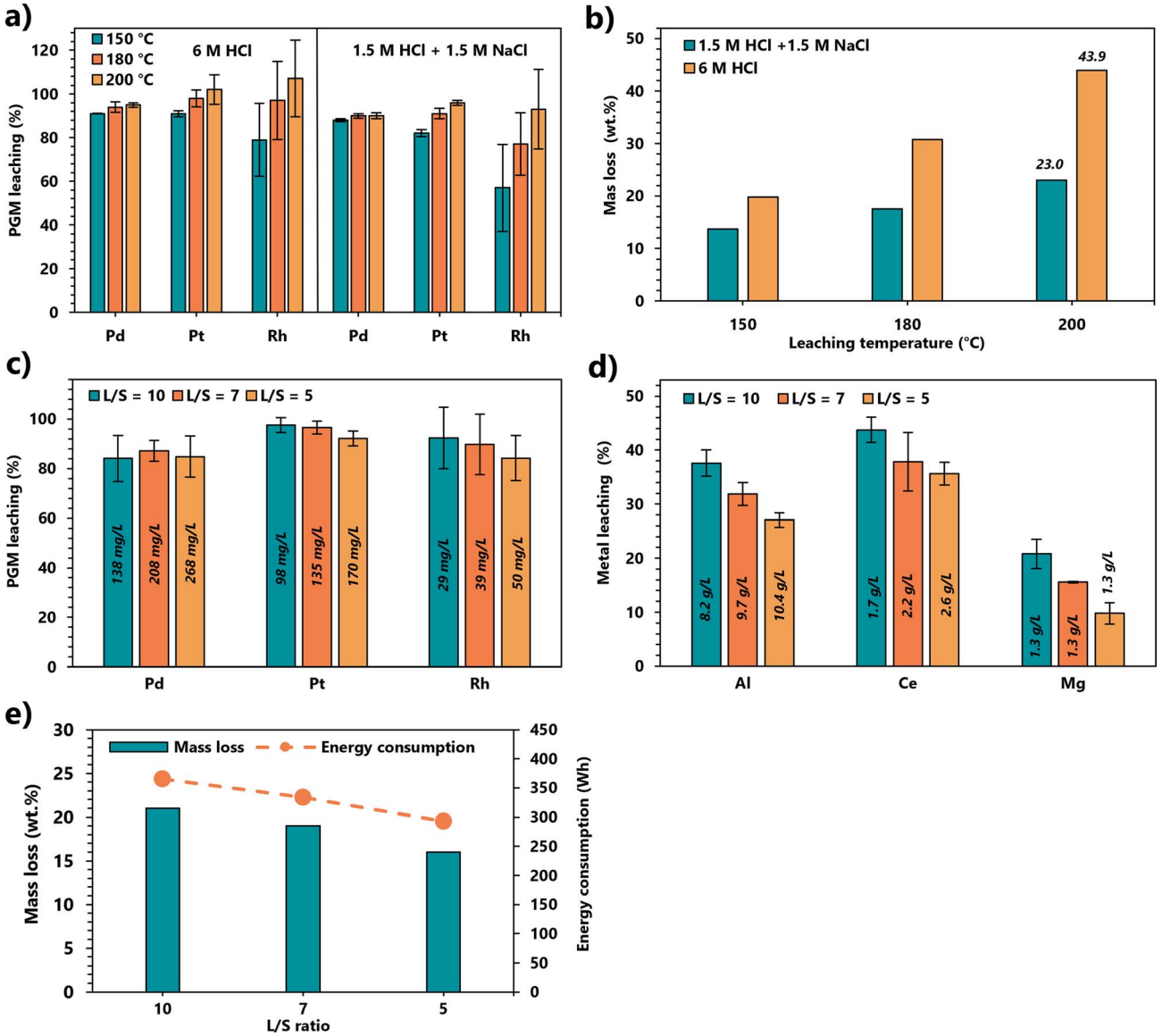


Fig. 1 Optimisation of microwave-assisted leaching (MWAL) parameters for PGM recovery. (a) PGM leaching efficiency at different temperatures and leaching compositions. (b) Solid mass loss as a function of temperature (liquid-to-solid ratio, L/S ratio = 10). (c) PGM leaching efficiencies at different L/S ratios at 200 °C (italic numbers indicate PGM concentration in the leachate). (d) Co-leaching of major matrix elements (Al, Ce, Mg) under the same conditions. (e) Correlation between total mass loss and energy consumption as function of L/S ratio at 200 °C.

The PGM-rich leachates obtained under these optimised MWAL conditions were subsequently subjected to GDEx for the selective recovery of PGM.

### 3.3. Gas-diffusion electrocrystallization (GDEx) optimisation

Following MWAL, the GDEx process was employed to recover the PGMs from leachates generated using two different leaching systems: 1.5 M HCl + 1.5 M NaCl and 6 M HCl, both conducted at 200 °C and a L/S ratio of 10.

The comparative performance of the GDEx process under both leaching systems is summarised in Table 1, with a detailed visual representation provided in Fig. 2 for the 1.5 M HCl + 1.5 M NaCl leachate. The results demonstrate the high efficiency and selectivity of GDEx for the recovery of PGMs from complex multielement leachates. These solutions contained more than 27 different chemical elements, with major matrix components including Al, Fe, Ce, La, Zn, Mg, Ca, Sr, and Nd. Some matrix element concentrations, particularly Al, reached values as high as 11 g $L^{-1}$ (Tables S4–S6; SI-IV, Section 4.1), whereas PGM concentrations ranged from 20 to 270 mg $L^{-1}$. Despite the compositional complexity and the large excess of matrix elements relative to PGMs, the GDEx process consistently achieved near-complete PGM removal, with yields approaching 100% metal conversion efficiency (solution-to-solid phase) across all tested current densities (10 mA $cm^{-2}$ to 200 mA $cm^{-2}$).

The high selectivity can be rationalised by the marked difference in thermodynamic reducibility between PGM

Table 1 GDEx metal extraction performance for the different MWAL leaching solutions at different current densities

| | Leaching solution: 1.5 M NaCl + 1.5 M HCl | | | Leaching solution: 6 M HCl | | |
|---|---|---|---|---|---|---|
| Conditions | 10 mA $cm^{-2}$ | 40 mA $cm^{-2}$ | 200 mA $cm^{-2}$ | 10 mA $cm^{-2}$ | 40 mA $cm^{-2}$ | 200 mA $cm^{-2}$ |
| Metal removal (%) | Pd: 100<br>Pt: 98.7<br>Rh: 98.5 | Pd: 95.5<br>Pt: 99.2<br>Rh: 95.5 | Pd: 100<br>Pt: 100<br>Rh: 100 | Pd: 98.7<br>Pt: 86.4<br>Rh: 50.9 | Pd: 96.9<br>Pt: 88.1<br>Rh: 31.6 | Pd: 96.2<br>Pt: 94.0<br>Rh: 39.4 |
| Average removal rate (mg $L^{-1}$ $min^{-1}$ $cm^{-2}$) | 0.18 ± 0.03 | 0.25 ± 0.03 | 0.57 ± 0.07 | 0.10 | 0.22 | 0.48 |
| Final pH | < 0 | 0.14 ± 0.02 | 0.42 ± 0.02 | < 0 | < 0 | < 0 |
| Cathode potential ($V_{Ag/AgCl}$) | −0.29 ± 0.02 | −0.35 ± 0.02 | −0.60 ± 0.05 | −0.25 ± 0.02 | −0.36 ± 0.04 | −0.49 ± 0.02 |
| Cell voltage (V) | 1.44 ± 0.03 | 1.62 ± 0.2 | 3.45 ± 0.11 | 1.38 ± 0.03 | 1.48 ± 0.02 | 2.94 ± 0.04 |
| Charge density (C $mg_{PGM}^{-1}$) | 32.1 ± 0.1 | 97.2 ± 0.1 | 205 ± 0.1 | 58.2 | 107.1 | 247.9 |
| Energy (kWh $kg_{PGM}^{-1}$) | 15 ± 2 | 44 ± 7 | 202 ± 3 | 23 | 44 | 203 |

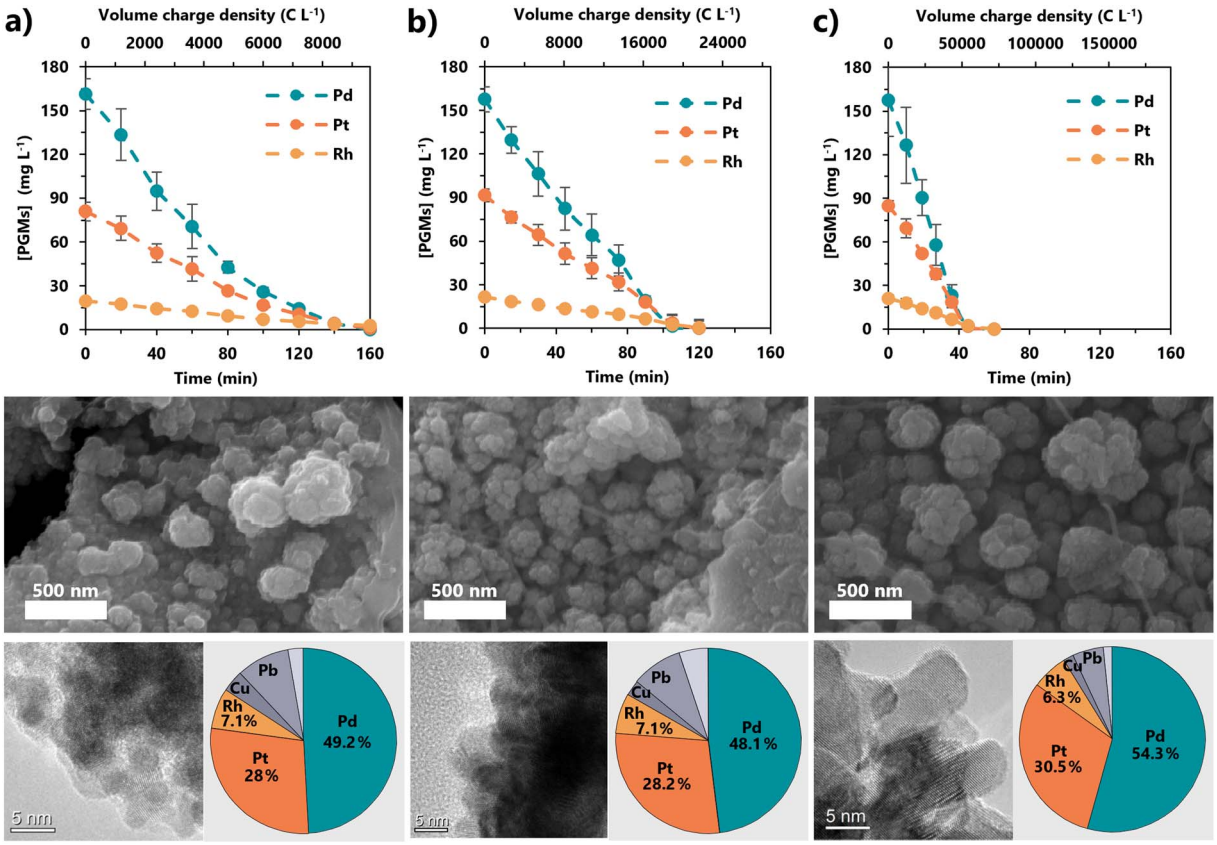


Fig. 2 GDEx treatment of the MWAL leachates under different current densities: (a–c) evolution of Pd, Pt, and Rh concentrations in the 1.5 M HCl + 1.5 M NaCl MWAL leachate during GDEx at (a) 10 mA $cm^{-2}$, (b) 40 mA $cm^{-2}$, and (c) 200 mA $cm^{-2}$, with corresponding SEM and TEM images of the recovered nanoparticles and pie charts showing their elemental composition.

chloride complexes and the major matrix elements present in the leachates. Under $CO_2$-fed GDEx conditions, electrogenerated $H_2$ and CO act as mild reducing agents. For PGM chloro-complexes, reduction to the metallic state by $H_2$ and/or CO is thermodynamically favourable, as indicated by the negative Gibbs free energy values calculated by the corresponding reactions (SI-III). In contrast, analogous reduction reactions involving main matrix elements are not thermodynamically favourable under the same conditions. Selectivity is further reinforced by the GDEx operating environments. Gas evolution and mass-transport limitations at the gas-diffusion electrode suppress conventional electrodeposition of less noble metals, while $CO_2/HCO_3^-$ buffering and the acidic bulk pH limit hydroxide precipitation of matrix elements.

While the thermodynamic framework explains the preferential recovery of PGMs over the matrix elements, the extent and rate of PGMs removal are governed by the applied operating conditions. As shown in Fig. 2, increasing the current density

accelerates the precipitation and removal efficiencies of PGMs. This is attributed to the enhanced *in situ* generation of reducing gases ($H_2$ and CO), which promote faster reaction kinetics as their concentration in the electrolyte bulk increases. However, this also leads to a higher energy consumption per unit mass of recovered metal (Table 1), suggesting that a significant fraction of the electrogenerated gases remains unreacted and is thus lost from the system. These findings underscore the need for a balanced optimisation approach that maintains high recovery efficiency while minimising energy input. Critical process parameters, such as current density, gas utilisation, and electrode surface area, must be carefully tuned in relation to the target processing capacity and operational constraints to identify the most energy- and resource-efficient operating conditions. The broader implications for process design and energy demand are further discussed in the following sections.

Table 1 shows that both the 6 M HCl and the 1.5 M HCl + 1.5 M NaCl leachates achieved similar PGM precipitation efficiencies and energy consumption, enabling complete and selective metal recovery. However, under the more aggressive 6 M HCl conditions, Rh recovery was slightly less effective. Moreover, the highly acidic environment led to significant corrosion of the stainless-steel mesh used in the GDE, as evidenced by the increased concentrations of Fe, Ni, Cr, and Mn compared to their initial values in the leachate (Table S7; SI-IV, Section 4.2). Although GDE corrosion was mitigated at 200 mA $cm^{-2}$ due to enhanced cathodic protection, it remained substantial. In contrast, minimal corrosion was observed when using the 1.5 M HCl + 1.5 M NaCl system. The colour change of the leachates during GDEx (Fig. S4, SI-IV, Section 4.2) further supports these findings: the 1.5 M HCl + 1.5 M NaCl leachate turned transparent upon PGM removal, while the 6 M HCl solution turned green, indicating GDE corrosion.

The products recovered from the treatment of the 1.5 M HCl + 1.5 M NaCl leachate *via* the GDEx process were further characterised, as shown in Fig. 2. The materials consisted of NPs of approximately 5 nm in size (TEM images), which tended to agglomerate into larger clusters (SEM images). The chemical composition of the three precipitates (pie charts and Table S8; SI-IV, Section 4.2) was highly similar, with PGMs accounting between 83% and 91% of the total mass, with Cu and Pb identified as the primary impurities. XRD analysis confirmed their metallic nature (Fig. S5, SI-IV, Section 4.2), and STEM-EDXS analysis (Fig. S6 and Table S9; SI-IV, Section 4.2) revealed a homogenous distribution of Pt, Pd, and Rh within the NPs, indicating the formation of a ternary alloy.

After assessing the effects of current density and leachate composition, additional operational parameters were evaluated to optimise GDEx for PGM recovery. These included the $CO_2$ gas flow rate, cathode material, application of sonication, anolyte composition, and L/S ratio during the leaching process. The base case for comparison, detailed in Table S10 (SI-IV, Section 4.2), employed a $CO_2$ gas flow rate of 200 mL $min^{-1}$, an applied current density of 40 mA $cm^{-2}$, 5 M NaCl as anolyte, and a GDE incorporating a stainless-steel mesh. The corresponding leachate was produced using a L/S ratio of 10 during the MWAL step. These conditions were chosen to investigate strategies for maximising PGM recovery, minimising energy consumption, and improving system stability.

As shown in Table 2 and Fig. S7 (SI-IV, Section 4.2), several key findings emerged. Reducing the $CO_2$ gas flow rate from 200 to 20 mL $min^{-1}$ did not compromise PGM recovery or increase energy consumption (Fig. S7b; SI-IV, Section 4.2), implying a more efficient gas utilisation. Transitioning to a flow-through (FT) gas regime and applying sonication, either individually or in combination, further enhanced PGM recovery rates (Fig. S7c and d; SI-IV, Section 4.2), likely due to improved mass transfer and reduced diffusion limitations. However, sonication significantly increased energy consumption, reaching 545 kWh per kg of PGMs. Notably, the FT configuration also reduced $CO_2$ usage to as low as 5 mL $min^{-1}$. Substituting the 5 M NaCl anolyte with 3 M $Na_2SO_4$ had no adverse effect on PGM recovery (Fig. S7e; SI-IV, Section 4.2) but eliminated chlorine gas formation, addressing a key environmental concern.

Two strategies were investigated to mitigate cathode corrosion, particularly affecting the stainless-steel mesh used in the

Table 2 GDEx metal extraction performance at different operating conditions ($CO_2$ flow regime and flow rate, sonication, anolyte composition, and GDE material). Default conditions: 40 mA $cm^{-2}$, flow-by (200 mL $min^{-1}$), VITO-CoRE® GDE with stainless steel mesh, and liquid-to-solid ratio (L/S) of 10 in the leaching process. The catholyte and anolyte volumes were 100 and 250 mL, respectively, and the electrolyte recirculation flow rate was 100 mL $min^{-1}$ for all cases

| Conditions | Default conditions | $CO_2$ – 20 mL $min^{-1}$ (FB) | $CO_2$ – FT | Sonication | Anolyte $Na_2SO_4$ | GDE-Ti mesh | L/S = 5 |
|---|---|---|---|---|---|---|---|
| Metal removal at $t$ = 120 min (%) | Pd: 95.5<br>Pt: 99.2<br>Rh: 95.5 | Pd: 95.8<br>Pt: 93.6<br>Rh: 87.5 | Pd: 100<br>Pt: 100<br>Rh: 100 | Pd: 100<br>Pt: 100<br>Rh: 89 | Pd: 100<br>Pt: 100<br>Rh: 96.8 | Pd: 100<br>Pt: 98.7<br>Rh: 94.9 | Pd: 100<br>Pt: 100<br>Rh: 100 |
| Average removal rate (mg $L^{-1}$ $min^{-1}$ $cm^{-2}$) | 0.25 | 0.21 | 0.33 | 0.33 | 0.26 | 0.27 | 0.72 |
| Cathode potential (V) | −0.35 ± 0.02 | −0.42 ± 0.02 | −0.40 ± 0.02 | −0.38 ± 0.01 | −0.51 ± 0.02 | −0.43 ± 0.02 | −0.66 |
| Anode potential + Σ(IR) (V) | 1.27 ± 0.01 | 1.89 ± 0.05 | 1.22 ± 0.17 | 1.31 ± 0.01 | 2.42 ± 0.09 | 1.24 ± 0.02 | 1.24 |
| Cell voltage (V) | 1.62 ± 0.2 | 2.31 ± 0.06 | 1.62 ± 0.17 | 1.69 ± 0.02 | 2.93 ± 0.11 | 1.67 ± 0.03 | 1.90 |
| Charge density (C $mg_{PGM}^{-1}$) | 97.2 | 115.2 | 72.3 | 73.0 | 91.0 | 89.0 | 33.3 |
| Energy GDEx (kWh $kg_{PGM}^{-1}$) | 44.4 | 74.5 | 32.4 | 34.0 (+545.1 sonication) | 73.9 | 41.4 | 17.5 |

GDE. As previously noted, increasing the current density provides cathodic protection, thereby reducing corrosion. However, this approach entails higher energy consumption and reduced operational flexibility. To address this, the replacement of the stainless-steel mesh with Ti was evaluated. Ti offers superior corrosion resistance in harsh environments, including acidic and brine solutions, making it a promising alternative.[36] Although it is intrinsically less active toward hydrogen evolution, its electrochemical performance and chemical stability can be significantly enhanced with a carbon-based coating, as implemented in this study. This strategy was validated by the results shown in Fig. S8 (SI-IV, Section 4.2), which demonstrated comparable hydrogen evolution performance between Ti and stainless steel meshes. Significantly, replacing stainless steel with Ti in the GDE effectively prevented corrosion without compromising PGM recovery (Table 2 and Fig. S7f; SI-IV, Section 4.2), thereby enhancing electrode durability.

Additionally, different L/S ratios during MWAL were evaluated for their impact on the subsequent GDEx process. A lower L/S ratio of 5, previously shown to yield leachates with higher metal concentrations, also significantly impacted GDEx performance. As shown in Table 2, it led to higher recovery rates and reduced energy consumption. However, the increased metal content also elevated the resulting leachate pH (0.61 *vs.* −0.13 for L/S = 10), raising the risk of co-precipitating non-targeted matrix elements during GDEx. Given that the electrochemical generation of $H_2$ and CO further increases the catholyte pH, processing L/S = 5 leachates could result in pH values exceeding 2 (Fig. S9; SI-IV, Section 4.2), triggering the precipitation of elements such as Al, Fe, Si, and Ce (Table S11; SI-IV, Section 4.2). To prevent this, a continuous pH adjustment protocol was implemented to maintain the pH below 1, ensuring selective PGM recovery as illustrated in Fig. S10 (SI-IV, Section 4.2).

### 3.4. MWAL-GDEx integration for leachate reuse

The integration of MWAL with GDEx, illustrated in Fig. 3a, was explored as a strategy to enhance the sustainability of the proposed PGM recovery pathway. This approach involved reusing the GDEx effluent (*i.e.*, the PGM-depleted leachate) as the leaching solution (lixiviant) in subsequent MWAL steps. The goal was to reduce water and reagent consumption (HCl and NaCl), minimise waste generation, and potentially improve the selectivity for PGMs. All tests were conducted at a L/S ratio of 10.

As shown in Fig. 3b and c, the recycled leachate achieved PGM extraction efficiencies (relative deviation of <15%) comparable to those obtained using fresh leaching solutions, even after three consecutive MWAL-GDEx cycles. To maintain consistent leaching performance, the pH of the recycled lixiviant was adjusted with 3% v/v HCl (0.36 M) to match that of the original solution (1.5 M HCl).

Fig. 3b and c also reveal a gradual decrease in the dissolution of matrix elements (*i.e.*, Al, Ce, Fe, and Mg) over successive cycles. This corresponds with a decline in the overall mass loss of the automotive catalyst material (Fig. 3c), suggesting that the leachate becomes progressively saturated with non-PGM elements. As the solubility of their chloride species is approached, the leaching yield of these matrix elements diminishes. In contrast, PGM extraction remains stable owing to the higher stability and solubility of their chloro-complexes in the lixiviant.

Finally, Fig. 3d highlights the robustness of the GDEx process in selectively recovering PGMs from the recycled leachates, consistently achieving metal conversion efficiencies above 95% for all three PGMs, across all three cycles. These findings demonstrate the technical feasibility of closed-loop leachate reuse and its potential to reduce the environmental impact of the overall recovery process.

### 3.5. Electrocatalytic application of GDEx-Recovered PGM nanoparticles in methanol oxidation

One of the distinguishing features of the GDEx process is that the PGMs are recovered as nanoparticles (NPs). To explore value-added applications beyond metal recovery, the GDEx-recovered PGM NPs were directly evaluated as electrocatalysts for fuel cell reactions, with a focus on the methanol oxidation reaction (MOR). Direct methanol fuel cells (DMFCs) are attractive for powering portable electronics, with Pt being the benchmark catalyst for MOR. However, Pt suffers from poisoning by adsorbed CO ($CO_{ads}$), a key intermediate in MOR, which hinders its commercial viability.[33] Alloying Pt with other metals has been proposed as a strategy to improve CO tolerance. Multimetallic Pt-based alloys, such as Pt–Pd–Rh alloy NPs, similar in composition to the GDEx-recovered NPs, have demonstrated enhanced MOR activity compared to their mono- or bimetallic counterparts due to synergistic effects.[37]

The electrochemical properties of the GDEx-recovered PGM NPs, obtained from MWAL leachates (1.5 M HCl + 1.5 M NaCl with L/S ratio of 10) at 10 mA $cm^{-2}$, 40 mA $cm^{-2}$, and 200 mA $cm^{-2}$, were characterised in Ar-saturated 0.5 M $H_2SO_4$ at room temperature. For comparison, a commercial 20 wt% Pt/C catalyst was used as a benchmark. The cyclic voltammograms (CVs) (Fig. S11, SI-IV, Section 4.3) exhibited the characteristic hydrogen adsorption–desorption region (between 0.050 and 0.350 V *vs.* RHE), confirming Pt-like surface behaviour. Electrochemical surface area (ECSA) values, normalised to Pt and total PGM content, are presented in Table 3. Notably, the ECSA increased with higher GDEx current density, which also correlates with a higher Pt content at the nanoparticle surface (Table S9), resulting in more electrochemically active sites for hydrogen adsorption. This behaviour likely arises from differences in the reduction mechanisms of the PGM precursors during GDEx, although a detailed mechanistic analysis lies beyond the scope of this work.

MOR activity was evaluated in Ar-saturated 0.5 M $H_2SO_4$ + 1.0 M methanol; the current density at the peak potential was normalised to the Pt or total PGM loading to calculate the mass activity (MA) and to the ECSA to determine the specific activity (SA), as shown in Table 3 and Fig. S12 (SI-IV, Section 4.3). As the same metal loading term is used in both the MA and ECSA calculations, this factor cancels out in the expression for SA (See SI-II, Section 2.3); consequently, the specific activity is

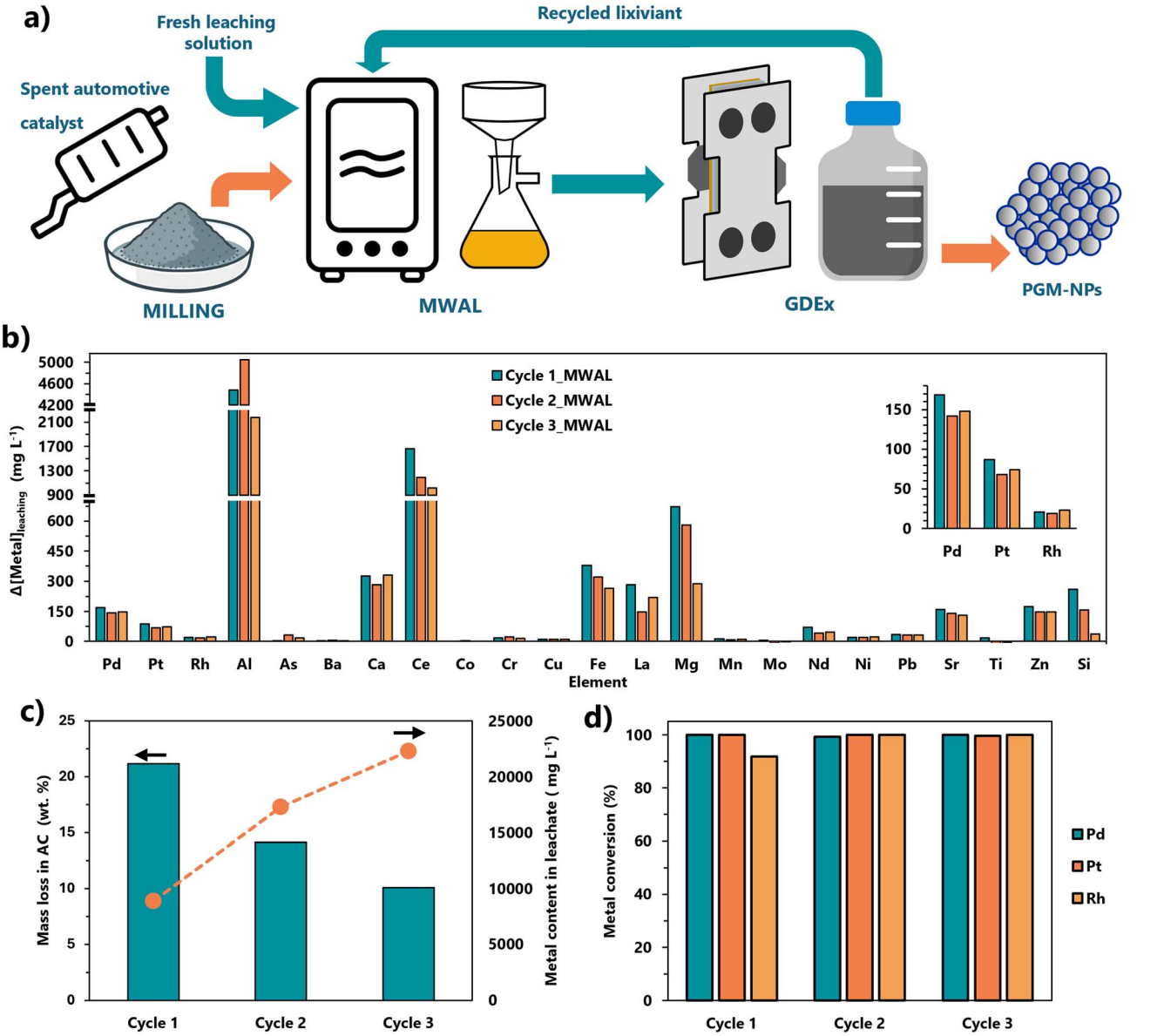


Fig. 3 Performance of the integrated MWAL-GDEx process over three leachate recycling cycles. (a) Schematic representation of the coupled MWAL-GDEx system, showing the recycling of the leaching solution between both steps. (b) Variation in dissolved metal concentrations (Δ[metal]) after each MWAL cycle, showing the progressive enrichment of the leachate. (c) Decrease in solid mass after leaching and corresponding increase in total dissolved metal content upon recirculation. (d) Recovery efficiency of Pt, Pd and Rh by GDEx across consecutive cycles.

Table 3 Electrochemical active surface area (ECSA), mass activity (MA), and specific activity (SA) for methanol oxidation of the PGM NPs recovered with the GDEx process from spent automotive catalyst leachates

| | Normalised to Pt content | | Normalised to PGM content | | |
|---|---|---|---|---|---|
| Sample | ECSA ($m^2\ g^{-1}$) | MA ($mA\ mg^{-1}$) | ECSA ($m^2\ g^{-1}$) | MA ($mA\ mg^{-1}$) | SA ($mA\ cm^{-2}$) |
| 10 $mA\ cm^{-2}$ | 17.2 ± 1.8 | 56.0 ± 9.3 | 3.1 ± 0.3 | 10.2 ± 1.7 | 0.33 ± 0.05 |
| 40 $mA\ cm^{-2}$ | 48.5 ± 9.0 | 96.6 ± 15.7 | 9.1 ± 1.7 | 18.1 ± 2.9 | 0.20 ± 0.03 |
| 200 $mA\ cm^{-2}$ | 57.3 ± 5.5 | 241.7 ± 32.1 | 11.4 ± 1.1 | 48.1 ± 6.4 | 0.42 ± 0.06 |
| Pt-Carbon | 47.9 ± 1.2 | 340 ± 26.0 | — | — | 0.71 ± 0.06 |

independent of whether Pt or total PGM loading is applied, and only a single value is reported. Among the GDEx-recovered materials, the NPs produced at 200 $mA\ cm^{-2}$ exhibited the highest overall catalytic performance toward MOR, with both MA (247.1 $mA\ mg_{Pt}^{-1}$) and SA (0.42 $mA\ cm^{-2}$) reaching their maximum values. Although this activity remained lower than

that of commercial Pt/C, which showed an MA of 340 mA $mg_{Pt}^{-1}$ and SA of 0.71 mA $cm^{-2}$, the GDEx recovered NPs displayed clear activity without additional purification or post-synthesis optimisation. The improved performance of the 200 mA $cm^{-2}$ sample is consistent with its larger ECSA and is associated with the higher Pt surface content (Table S9; SI-IV, Section 4.3), which enhances the number and intrinsic activity of accessible catalytic sites.[28,29]

Accelerated durability was assessed over 1000 CV cycles (Fig. S12c, SI-IV, Section 4.3). For the NPs produced at 10 mA $cm^{-2}$ and 40 mA $cm^{-2}$, the current density increased during the initial ~100 cycles, whereas the sample obtained at 200 mA $cm^{-2}$ reached its peak around 400 cycles. This initial enhancement is attributed to progressive surface cleaning or dynamic restructuring of the NP surface.[38,39] Beyond this peak, all samples exhibited a gradual decline in activity. After 1000 cycles, the MA of the 200 mA $cm^{-2}$ sample retained approximately 85% of its maximum value, while the other two materials maintained around 50%. In contrast, commercial Pt/C retained only 26% of its activity after the same durability protocol, indicating that the GDEx-recovered multimetallic NPs, although less active initially than Pt/C, exhibit superior stability under the tested MOR conditions. When benchmarked against literature, the 200 mA $cm^{-2}$ GDEx-recovered NPs showed comparable activity to selected pure Pt nanomaterials, such as Pt NP assemblies (MA = 239 mA $mg_{Pt}^{-1}$)[40] and high-surface-area Pt nanotubes (MA = 200 mA $mg_{Pt}^{-1}$).[41] Their activity was lower than that of commercial Pt/C and literature-reported Pt–Pd–Rh catalysts deliberately engineered for MOR, including Pt–Pd–Rh mesoporous nanospheres (SA = 1.41 mA $cm^{-2}$)[37] and Pt–Rh–Pd alloy nanochains (SA of 1.48 mA $cm^{-2}$).[42] Nevertheless, their higher durability compared with Pt/C highlights a potential advantage of the GDEx-recovered multimetallic composition. Importantly, these results were obtained without additional pretreatment (*e.g.*, milling to reduce agglomeration), suggesting potential for further performance improvements. These findings do not aim to establish the GDEx-recovered materials as state-of-the-art MOR catalysts but rather provide proof of concept that GDEx can recover PGMs directly as functionally active electrocatalytic nanoparticles. This demonstrates a potential upcycling pathway beyond conventional recycling routes based solely on producing enriched PGM intermediates for further refining.

### 3.6. Life cycle assessment (LCA)

This section presents the potential environmental impacts of PGM recovery from automotive catalysts *via* the combined use of sample milling, MWAL, and GDEx technologies (Fig. 4). Tables S12–S14 (SI-IV, Section 4.4) summarise the impacts by process stage (base case), disaggregated contributions, and scenario comparisons (base case *vs.* alternative scenarios). We complemented the deterministic results with a Monte Carlo

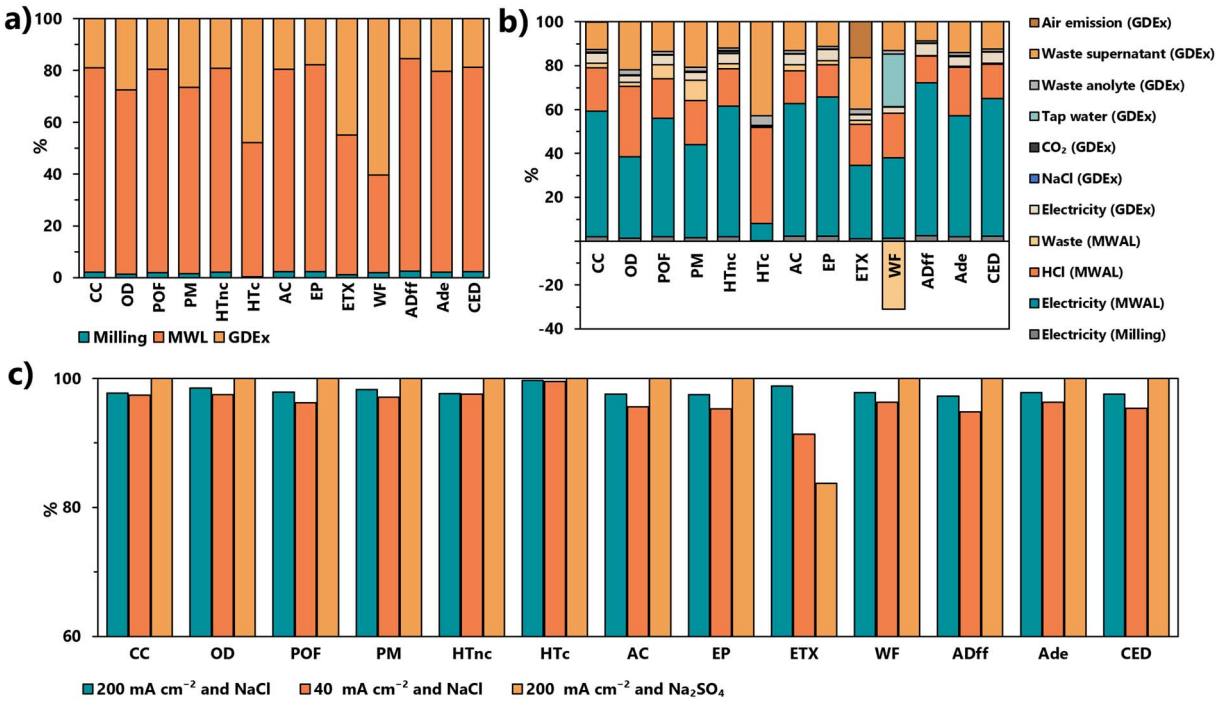


Fig. 4 Environmental performance of the integrated MWAL-GDEx process. (a) Contribution of each process stage to total environmental impacts under the base case scenario (200 mA $cm^{-2}$ and NaCl electrolyte). (b) Disaggregated environmental impacts across all categories for the base case scenario. (c) Comparison between the base case and alternative scenarios across impact categories. The *y*-axis is truncated (60–100%) to emphasise relative differences among impact categories. Impact categories include: climate change (CC), ozone layer depletion (OD), photochemical ozone formation (POF), particulate matter formation (PMF), human toxicity-cancer (HTc), human toxicity-non-cancer (HTnc), acidification (AC), eutrophication (EP), freshwater ecotoxicity (ETX), water footprint (WF), abiotic resource depletion-elements (ADe), abiotic resource depletion-fossil fuels (ADff), and cumulative energy demand (CED).

uncertainty analysis. As expected for attributional LCA, which draws on heterogeneous datasets, uncertainty is higher for ETX, HT-c, HT-nc, and WF. These impact categories are therefore interpreted qualitatively/indicatively, while the hotspot diagnosis and scenario ranking rely primarily on categories with lower relative uncertainty (*e.g.*, CC, CED, and AC). A hotspot analysis was conducted to identify opportunities for improvement (Table S12; SI-IV, Section 4.4).

Based on the results shown in Fig. 4a, MWAL exhibits the highest contribution to the overall impact, accounting for an average of 70.7%, both in total and across individual impact categories. GDEx ranks as the second-largest contributor, representing an average of 27.4%, while the impact of sample milling is negligible.

To further understand the sources of environmental impact, the results were disaggregated by input/output contributions (Fig. 4b). This indicates that electricity consumption in MWAL is the single largest contributor, responsible for approximately 49.2% of the total average impact. In contrast, the second-largest contributor is the HCl used in the MWAL process, averaging 20.7% of the impacts, followed by the neutralisation and precipitation treatment modelled for the GDEx waste supernatant, which represents 16.8% of the total impact.

The environmental assessment highlights energy consumption as the primary contributor. Therefore, improving energy efficiency must be the primary focus for future developments. While laboratory-scale experiments inherently demand more energy, upscaling offers significant opportunities, as larger systems are typically more energy-efficient than laboratory equipment. In the LCA simulation, a heat exchanger—proposed in the pilot-scale design of the PEACOC project—was integrated to recover heat from the outgoing leachate of the MW reactor, allowing pre-heating of the incoming feed and achieving an estimated 30% reduction in heating demand. Further research could evaluate additional heat recovery strategies at pilot scale, as well as other energy-saving measures, to lower overall energy requirements. Using renewable electricity instead of the European electricity mix—which includes fossil sources—results in an average reduction of 43% across all impact categories, and a 60% reduction specifically in the CC category.

The second major contributor to the process is HCl consumption in MWAL. Reducing the use of this reagent—through process adjustments and potential partial substitution—was already an objective during the laboratory phase, and LCA results were obtained under the laboratory scale optimised conditions. Nevertheless, the full potential should be further investigated and validated during process scale-up.

In addition to these two key aspects, improvements already tested at laboratory scale, such as the use of lower chemical concentrations and shorter reaction times, also contributed to reducing the footprint. These combined strategies substantially enhance the sustainability of the MWAL process on an industrial scale.

For GDEx, additional impact reductions may require alternative treatment approaches, as effluent recirculation is already optimised within the process. Nonetheless, further mitigation could be achieved by exploring alternative waste treatment strategies, particularly to minimise the impacts associated with the neutralisation and precipitation steps.

From an experimental standpoint, several strategies were tested to optimise the GDEx base case scenario in terms of both environmental and technoeconomic performance. First, the effect of reducing the current density from 200 mA $cm^{-2}$ to 40 mA $cm^{-2}$ was evaluated. This adjustment led to decreased energy consumption but required a higher $CO_2$ flow rate and an increased number of unit cells (from 6 to 16) as discussed in the TEA. As shown in Fig. 4c, this scenario offered a modest environmental improvement, reducing the average overall impact by approximately 2.6%.

Second, the substitution of NaCl in the anolyte with $Na_2SO_4$, aimed at eliminating $Cl_2$ gas formation, was also assessed. While this approach avoided $Cl_2$ emissions, the overall average impact increased by 2.4% compared to the base case, except for ETX, which decreased by 15.3% due to the elimination of chlorine gas. However, given the high uncertainty shown in this impact category, this specific result should be regarded as indicative rather than conclusive. This increase is attributed to higher power consumption and the greater quantities of $Na_2SO_4$ required, along with its associated environmental impact.

In essence, these findings highlight two main levers (i) the importance of targeting energy efficiency (equipment and heat integration) in the MWAL step and (ii) GDEx effluent management to improve the overall sustainability of the process. While alternative configurations provided modest gains, combining L/S optimisation, closed-loop leachate reuse, reagent optimisation, and low-carbon electricity offers the most significant pathway to footprint reduction.

### 3.7. Techno-economic assessment (TEA)

A TEA was conducted to evaluate the scalability and profitability of the integrated MWAL-GDEx process for PGM recovery, aligned with the PEACOC project KPIs. The model considered the treatment of 50 L $h^{-1}$ of leachate, based on laboratory-optimised parameters: a L/S ratio of 5 in MWAL (with leaching efficiencies of Pt: 92.2 $\pm$ 3.0%; Pd: 84.8 $\pm$ 8.3% and Rh: 84.2 $\pm$ 9.1% according to experimental results), a flow-through $CO_2$ regime, and 200 mA $cm^{-2}$ in the GDEx unit. This setup corresponds to a feed of 7.4 spent automotive catalysts per hour (monolith-only mass approximately 1.5 kg each; total: 11.1 kg $h^{-1}$) and an annual PGM-NP yield of approximately 224 kg. The assumed product purity of approximately 90% w/w is based on the GDEx product composition shown in Fig. 2 and quantified in Table S8 (SI-IV, Section 4.2). Although smaller than centralised pyrometallurgical facilities, this scale reflects modular deployment near dismantling hubs, with potential replication advantages. The complete list of assumptions for the TEA is shown in Table 4. A full mass and energy balance of the optimised and integrated process was carried out and is presented in Fig. 5a, aiming to minimise waste streams and reduce feedstock consumption (*e.g.*, water and NaCl, as indicated by crossed-out streams in Fig. 5a). Additionally, the recirculation of the PGM-depleted solution back to the MWAL stage was

Table 4 Assumptions considered in the techno-economic assessment

| Parameter | Value/description |
|---|---|
| Operation duration | 330 days per year |
| Time horizon (years) | 10 |
| Process flow rate (L $h^{-1}$) | 50 |
| Anolyte flow rate (L $h^{-1}$) | 20 |
| PGM content in in spent automotive catalyst monolith (mg $kg^{-1}$) | Pt: 943, Pd: 1700, Rh: 272 |
| PGM leaching efficiency in MWAL step, L/S = 5 (%) | Pt: 92.2, Pd: 84.8, Rh: 84.2 |
| PGM recovery efficiency, GDEx (%) | 95 (based on dissolved PGM fraction) |
| PGM settling-washing efficiency (%) | 95 |
| PGM purity in product after GDEx step (wt%) | 90 |
| Current density in the GDEx stack (mA $cm^{-2}$) | 200 |
| Input feed cost (€ per spent automotive catalytic converter) | 172.8 |
| Average catalyst monolith mass per automotive catalyst unit (kg per $unit_{AC}$) | 1.5 |
| Electricity cost (€ per MWh) | 200 |
| FT-$CO_2$ gas flow regime (L per h per cell) | 7.8 |
| PGM market price (€ per kg) | Pt: 68 485, Pd: 52 195, Rh: 283 574 |
| Selling price (to smelter) of PGM-NP product (€ per kg) | 67 231 |
| Lang factor for CAPEX | 3 |
| Uncertainty factor applied to CAPEX and OPEX (%) | 20 |
| General maintenance (contribution to OPEX) (%) | 10% of preliminary OPEX (excluding spent AC cost) |

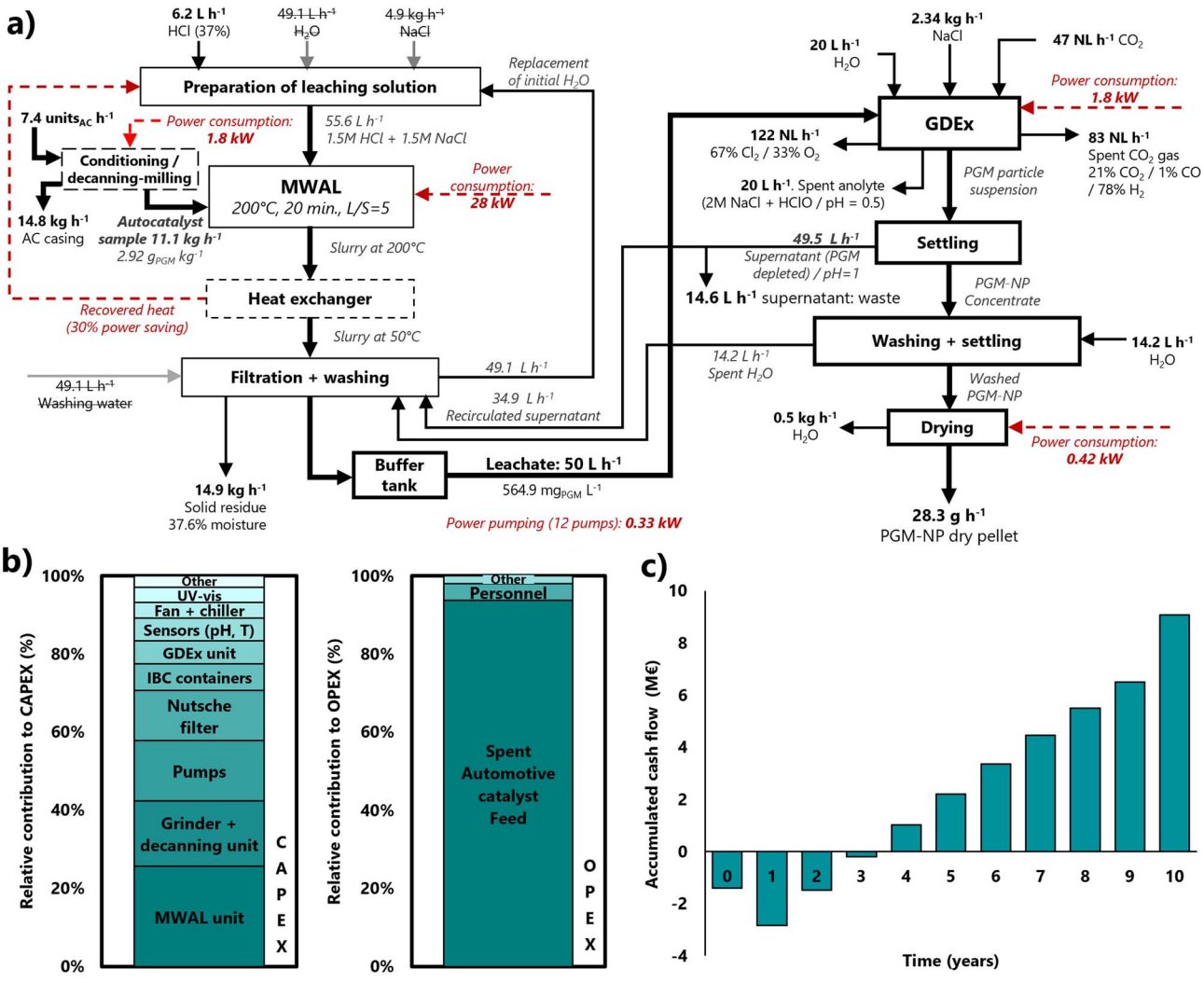


Fig. 5 Techno-economic performance of the integrated MWAL-GDEx process. (a) Mass and energy balance of the integrated process (MWAL operated at liquid-to-solid ratio, L/S ratio = 5; GDEx at 200 mA $cm^{-2}$). (b) Breakdown of the capital (CAPEX) and operational (OPEX) expenditures. (c) Cumulative cash flow and net present value (NPV) of the integrated process.

considered to enhance resource efficiency, with its technical feasibility demonstrated in Section 3.4.

Based on the GDEx product composition and average January 2026 PGM prices (Pt: 2448 $ per troy oz or 68,49 k€ per kg; Pd: 1866 $ per troy oz or 52,20 k€ per kg; Rh: 10 138 per troy oz or 283.57 k€ per kg), the gross (theoretical) metal value of the recovered PGM blend is 70.77 k€ per kg. In the base scenario, the GDEx product was assumed to be sold to a smelter/refinery, representing a conservative and realistic lower-bound valorisation route. This assumption accounts for the fact that PGM-containing intermediates are generally not paid at their full theoretical metal value, because further assay, refining, recovery, handling, and commercial deductions are required. This base case therefore does not include any additional value associated with the demonstrated nanoparticle nature and electrocatalytic functionality of the GDEx product (which is considered separately in the favourable selling-price scenario). Accordingly, the selling price of the PGM blend product to a smelter was estimated at 67.23 k€ per kg, which includes a 5% deduction applied to the gross PGM value to account for typical refining fees for a high-grade PGM concentrate (*e.g.*, 90% w/w PGM content).[43]

Whole (as-received, canned) end-of-life automotive catalyst converters are typically traded at 40–50% of their contained PGM value, depending on PGM loading, vehicle type/age, and market fluctuations in PGM prices. This discount accounts for sampling/assaying, logistics, processing losses, and recycler/refiner margins. Based on a 1.5 kg monolith containing 4.37 g PGMs (1.41 g Pt, 2.55 g Pd, 0.41 g Rh; Section 3.1), we assumed a feed cost of 172.8 € per unit, corresponding to ~50% of the contained PGM value, which is a conservative estimate in line with reported market values for Euro V–VI passenger-vehicle catalysts.[44] The decanning, milling and homogenisation steps prior to leaching are explicitly included in the process mass and energy balance and in the TEA (Fig. 5a, Tables S15 and S16 in the SI-IV).

Based on 2025 data, European industrial electricity prices commonly range 100–200 € per MWh; we fix 200 € per MWh in the base case to capture potential volatility.[45]

The upscaled integrated process comprises seven semi-batch MWAL reactors in the base case. Each MWAL reactor was assumed to have a total volume of 1.5 L, with an effective filling volume of 1.2 L. Reactor sizing was based on the complete filling-to-filling operating cycle, including filling, microwave heating, dwelling, emptying, and preparation for the next cycle. This cycle was assumed to take approximately 8 min, corresponding to an effective treatment capacity of about 9 L $h^{-1}$ per reactor. Therefore, seven MWAL reactors provide sufficient installed capacity for the nominal 50 L $h^{-1}$ case, while thirteen reactors are required for the 100 L $h^{-1}$ case. The detailed sizing assumptions and corresponding CAPEX/OPEX breakdown are provided in the SI-IV, Section 4.5.

The MWAL step is followed by filtration to separate the non-leached monolith residue, mainly ceramic matrix material, from the PGM-bearing leachate. The filtered solid is washed to recover residual leachate retained in the wet residue, including remaining dissolved PGMs. To minimise fresh-water make-up, washing is performed using recirculated process streams, including PGM-depleted supernatant after GDEx/settling and spent wash water from downstream PGM-NP washing. The resulting wash streams are recirculated within the integrated process to reuse acidic/chloride-containing liquor in the leaching step (refer to Fig. 5). The clarified PGM-bearing leachate is then fed to the continuous GDEx unit.

The GDEx unit employs a six-cell stack, with each cell featuring electrodes with a surface area of 325 $cm^2$. This configuration is based on extrapolated performance data at a current density of 200 mA $cm^{-2}$, corresponding to a charge requirement of 25 252 C $L^{-1}$, as determined experimentally. To optimise material and energy efficiency, the reactor design incorporates shared anodes and gas chambers between adjacent cells. A mixed series-parallel electrical configuration is employed to balance voltage control and current distribution across the stack, ensuring a stable power supply during operation.

Capital and operational expenditures (CAPEX and OPEX) were estimated using a Lang Factor of 3, appropriate for processing plants with accounted construction, instrumentation, and indirect costs; and a 20% contingency to cover potential overruns. Under the baseline conditions (200 mA $cm^{-2}$), the CAPEX was estimated at 1.41 M€, OPEX at 13.00 M€ per year, and with annual revenues at 15.08 M€ per year, resulting in a 13.9% operating profit margin (Fig. 5b and c). A detailed cost breakdown is provided in Tables S15–S18 (SI-IV, Section 4.5). Notably, spent automotive catalyst feed accounts for ~94.4% of OPEX and represents an exogenous factor. An alternative configuration of operating GDEx at 40 mA $cm^{-2}$ (Fig. S13; SI-IV, Section 4.5) required 16 GDEx cells to deliver the 14 400 C $L^{-1}$ needed for PGM recovery at this current density, compared to the 200 mA $cm^{-2}$ six-cell stack baseline. This configuration leads to a modest increase in CAPEX (1.49 M€) and OPEX (13.08 M€ per year), mainly due to the larger number of unit cells in the electrochemical stack and peripherals, and higher $CO_2$ demand (140 L $h^{-1}$ *vs.* 47 L $h^{-1}$), despite lower per cell power input, respectively. In addition, the 200 mA $cm^{-2}$, six-cell configuration shows a lower environmental footprint (see LCA section) and is therefore adopted as the reference case.

The net present value (NPV) was used to assess the economic viability of the integrated MWAL-GDEx process, representing the difference between the present value of expected cash inflows and outflows over the project's lifetime. A positive NPV indicates returns that exceed capital costs. The analysis, based on the assumptions in Table S19 (SI-IV, Section 4.5), included CAPEX, OPEX, and projected revenues over a 10 year period, with a 3% annual inflation rate applied to adjust financial flows. The invested funds comprise the initial CAPEX at year 0 (start of the project) and the working capital requirement at year 1 (start of operations), taken as 20% of sales. At the end of the operating period (year 10), a residual value equal to 10% of CAPEX and the recovery of working capital were included, as summarised in Table S19 and reflected in the cash-flow structure reported in Table S20. The discount rate ($r$), equated to the weighted average cost of capital (WACC), was calculated at approximately 7% (refer to SI-II Section 2.5), which reflects the moderate to high-risk profile typical of the recycling sector. Under these

assumptions, the projected cumulative cash flows (Fig. 5c and Table S20 in SI-IV) yielded an NPV of 9.08 M€, a return on investment (ROI) of 645.0%, an internal rate of return (IRR) of 45.1%, and a four-year payback period, confirming the financial robustness and profitability potential of the proposed value chain. At break-even (NPV = 0), the base-case requires a PGM product price of 59.24 k€ per kg (13.29 M€ per year revenues) and limits the EoL converter cost to 197.86 € per unit.

Three alternative scenarios were evaluated to assess the economic sensitivity of the integrated MWAL-GDEx process (Table 5). These scenarios target the main economic drivers identified from the OPEX breakdown: spent automotive catalyst cost, treatment capacity, and product selling price. Electricity price variation was not selected as a primary TEA scenario because electricity contributes <0.5% of total OPEX under the present assumptions. A 10% increase in spent automotive catalyst cost (from 172.83 to 190.12 € per unit) raised the annual OPEX to 14.22 M€, reducing the IRR to 18.3% and ROI to 199.8%, and extended the payback period to eight years, indicating strong sensitivity to feedstock pricing. Doubling the treatment capacity to 100 L $h^{-1}$ increased CAPEX to 1.80 M€ and OPEX to 25.37 M€ per year, respectively, but substantially improved financial performance, with revenues reaching 30.16 M€ per year, an IRR of 62.5% and an NPV of 21.65 M€, highlighting the benefits of scale-up. Lastly, a +10% selling-price scenario for the synthesized PGM-NPs (from 67.23 to 73.96 k€ per kg) was evaluated to represent a potential functional-product pathway beyond the conservative smelter/refinery route. This scenario was included because product value directly affects profitability and because the GDEx product is a high-PGM-content Pt–Pd–Rh nanoparticle material with demonstrated electrocatalytic functionality, which may justify higher-value applications compared with conventional PGM-containing intermediates. The premium is bracketed by two bounds: the refiner netback in the base case (lower bound, PGM market value minus assay, homogenization, and refining charges as previously described) and (ii) the value of an application-grade catalyst product (upper bound). A 10% uplift is justified because the GDEx product meets key performance and specification criteria—~90 wt% PGM, ~5 nm alloyed Pt–Pd–Rh nanoparticles, and demonstrated electrocatalytic activity for niche market applications (*e.g.,* methanol oxidation with stable cycling, Section 3.5)—allowing direct use or minimal finishing and avoiding dissolution/refining steps. Under this conservative (≤10%) premium, the metrics improve to IRR = 78.5%, NPV = 16.71 M€, and ROI = 1187.8%. Among the scenarios evaluated, this case yields the highest break-even feedstock price (218.92 € per unit), *i.e.,* the greatest tolerance to increases in EoL converter cost.

Overall, the TEA demonstrates that the integrated MWAL-GDEx process is economically robust under conservative assumptions, with profitability primarily driven by feedstock costs and the market valuation of nanoparticle products. While smaller in scale than existing pyrometallurgical operations, the modular and electrified nature of the process provides resilience against feedstock volatility and an opportunity to target high-value catalytic applications.

### 2.5. Policy and regulatory trajectory for decentralised recovery

The results presented in this study not only validate the technical feasibility of a fully electrified MWAL-GDEx route but also align with ongoing policy debates on critical raw materials, recycling targets, and industrial resilience. The security of supply of PGMs is already a global policy priority, with governments advancing circularity strategies and regulatory frameworks to mitigate dependence on fragile, concentrated primary supply sources. Within the EU, instruments such as the critical raw materials act,[46] the end-of-life vehicle (ELV) directive,[47] and the waste shipment regulation[48] define strict requirements for the collection, handling, and cross-border transport of PGM-bearing materials. These rules ensure environmental

Table 5 Financial results of different scenarios alongside the base case (GDEx-leachate treatment flow rate of 50 L $h^{-1}$, spent automotive catalyst (AC) cost of 172.83 € per unit, and selling price of 90% w/w purity PGM product of 67.23 k€ per kg). Alternative scenarios include: (1) 10% higher cost of the automotive catalyst (190.12 € per unit), (2) 100 L $h^{-1}$ treatment capacity, and (3) 10% higher selling price of PGM product (73.96 k€ per kg, by targeting a suitable market that acknowledges the higher added value of synthesizing nanoparticles, *e.g.,* methanol fuel cells). CAPEX stands for capital expenditure, OPEX for operational expenditure, NPV for net present value, IRR for internal rate of return and ROI for return on investment. "Break-even product price" and "break-even feedstock price" denote, respectively, the minimum PGM selling price and maximum end-of-life (EoL) automotive catalyst (AC) cost at NPV = 0

| | Base case | (1) Spent AC cost 190.12 € per unit | (2) Treatment capacity: 100 L $h^{-1}$ | (3) Selling price 73.96 k€ per kg |
|---|---|---|---|---|
| CAPEX/M€ | 1.41 | 1.41 | 1.80 | 1.41 |
| OPEX/M€ per year | 13.00 | 14.22 | 25.37 | 13.00 |
| Revenues/M€ per year | 15.08 | 15.08 | 30.16 | 16.59 |
| NPV/M€ | 9.08 | 2.81 | 21.65 | 16.71 |
| IRR/% | 45.1 | 18.3 | 62.5 | 78.5 |
| ROI/% | 645.0 | 199.8 | 1203.7 | 1187.8 |
| Operating profit margin/% | 13.9 | 5.8 | 16.0 | 21.7 |
| Payback period/year | 4 | 8 | 3 | 2 |
| Break-even product price/k€ per kg | 59.24 (13.29 M€ per year) | 64.76 (14.52 M€ per year) | 57.70 (25.70 M€ per year) | 59.24 (13.29 M€ per year) |
| Break-even feedstock price/ € per $unit_{EoL\text{-}AC}$ | 197.86 | 197.86 | 202.67 | 218.92 |

safeguards and traceability. However, they also lock the system into large, centralised facilities and multi-actor logistics chains, where leakages and inefficiencies persist.

Taken with our LCA, the case for modular, electrified hydrometallurgical units is conditional rather than universal. While sitting close to dismantlers or pre-treatment centers can reduce transport distances, hand-offs, and leakage risk, our hotspot analysis shows that MWAL electricity demand and GDEx effluent neutralisation dominate the impacts. Decentralised deployment, therefore, improves sustainability only if (i) units are energy-efficient (optimised L/S, heat management, microwave duty-cycling), (ii) low-carbon, competitively priced electricity is available (grid or on-site renewables), and (iii) closed-loop leachate reuse/pH control minimises neutralisation burdens. Under these conditions—demonstrated in our scenarios with reduced energy per kg PGM and effluent recirculation—local units can remain fully compliant (permitting, wastewater, chain-of-custody, safety) and still deliver system benefits by capturing low-grade or dispersed streams that central facilities often miss. Absent these conditions (*e.g.*, carbon-intensive power, poor effluent management), decentralisation may shift rather than reduce impacts. Accordingly, policy that facilitates low-carbon power access, proportionate permitting for small plants, and clear custody/settlement rules would enable decentralised MWAL-GDEx to complement—not replace—central hubs.

Positioned within this regulatory and policy landscape, decentralised MWAL-GDEx units represent a trajectory for reconciling critical-material security with environmental protection and industrial competitiveness. By bridging the gap between fragmented collection and centralised refining, such mobile or satellite systems could complement existing infrastructure and help deliver on circular economy objectives.

# 4. Conclusions

This work demonstrates a fully electrified and modular route for recovering and upcycling platinum-group metals (PGMs) from end-of-life automotive catalytic converters by coupling microwave-assisted leaching (MWAL) with $CO_2$-fed gas-diffusion electrocrystallization (GDEx).

MWAL operated with 1.5 M HCl + 1.5 M NaCl ($T \leq 200$ °C, L/S $\leq$ 10) achieved ≥90% PGM leaching while limiting matrix co-dissolution at lower L/S. The subsequent GDEx step, run at room temperature over 10–200 mA $cm^{-2}$, delivered >95% solution-to-solid conversion of dissolved PGMs into ~5 nm Pt–Pd–Rh nanoparticles with ~83–91 wt% PGM purity. Power consumption varied from 15 to 202 kWh $kg^{-1}$, increasing with current density. Optimising the L/S ratio improved recovery kinetics and helped reduce energy input.

Recirculating the PGM-depleted GDEx effluent as MWAL lixiviant (L/S = 10) maintained PGM extraction efficiency after minor pH readjustment (pH = −0.18). Over three cycles, leaching became progressively more selective to PGMs, with reduced matrix dissolution as the recycled leachate became enriched in these species, while GDEx consistently delivered >95% conversion of Pt, Pd and Rh. This supports leachate recirculation as a practical lever to reduce reagent use, water demand, and waste.

As-recovered PGM nanoparticles acted directly as MOR electrocatalysts, reaching MA = 241.7 mA $mg_{Pt}^{-1}$ (or 48.1 mA $mg_{PGM}^{-1}$), SA = 0.42 mA $cm^{-2}$, and ~85% retention after 1000 cycles—showing that the process upcycles PGMs into value-added catalytic materials without post-treatments.

LCA identified MWAL electricity as the dominant hotspot (~half of average impacts), followed by GDEx effluent neutralisation. Modelled 30% heat recovery and the use of low-carbon electricity markedly reduces burdens (up to 60% in Climate Change). Additional improvements include optimised L/S, closed-loop leachate/pH control, and minimising $Cl_2$ generation *via* $Na_2SO_4$ anolyte where appropriate.

At a modular scale of 50 L $h^{-1}$ leachate throughput, TEA indicates economic viability under conservative assumptions (operating margin 13.9%, NPV = 9.08 M€, IRR = 45.1%, 4-year payback). Scaling up to 100 L $h^{-1}$ and/or valorisation of the nanoparticle product further strengthens returns, while profitability is sensitive to feedstock costs—typical for the sector.

Overall, MWAL-GDEx delivers a scalable, electrified route that closes the PGM loop while directly upgrading recovered metals into functional materials—linking circularity with decarbonisation and creating a credible pathway for compliant, decentralised recovery.

# Author contributions

Luis F. Leon-Fernandez: conceptualization; data curation; formal analysis; investigation; validation; visualization; methodology; writing – original draft; writing – review & editing. Frantisek Kukurugya: data curation; investigation; methodology; visualization; writing – original draft; writing – review & editing. Omar Martinez-Mora: data curation; formal analysis; investigation; visualization; methodology; writing – original draft; writing – review & editing. Stefanos Mourdikoudis: writing – review & editing. Lunjie Zeng: investigation; writing – review & editing. Maria M. Parascanu: formal analysis; investigation; visualization; methodology; writing – original draft; writing – review & editing. Aitana Saez: investigation; supervision; methodology; writing – review & editing. Jan Fransaer: supervision; writing – review & editing. Jeroen Spooren: conceptualization; funding acquisition; supervision; writing – review & editing. Xochitl Dominguez-Benetton: conceptualization; funding acquisition; methodology; supervision; writing – review & editing.

# Conflicts of interest

There are no conflicts to declare.

# Abbreviations

| | |
|---|---|
| ADT | Accelerated durability test |
| sADe | Abiotic resource depletion element |
| ADff | Abiotic resource depletion fossil fuel |
| AC | Acidification |
| CAPEX | Capital expenditure |
| CuUPD | Copper underpotential deposition |

| | |
|---|---|
| CRMs | Critical raw materials |
| CED | Cumulative energy demand |
| CP | Chronopotentiometry |
| CC | Climate change |
| CV | Cyclic voltammetry |
| DMFC | Direct methanol fuel cell |
| EBIT | Earnings before interests and taxes |
| ETX | Ecotoxicity |
| EoL | End-of-life |
| EDXS/EDS | Energy-dispersive X-ray spectroscopy |
| EU | European union |
| EP | Eutrophication |
| FU | Functional unit |
| GDEx | Gas-diffusion electrocrystallization |
| GDE | Gas-diffusion electrode |
| GCE | Glassy carbon electrode |
| HTc | Human toxicity – cancer |
| HTnc | Human toxicity – non-cancer |
| ICP-OES | Inductively coupled plasma optical emission spectroscopy |
| IRR | Internal rate of return |
| L/S | Liquid-to-solid ratio |
| LCA | Life cycle assessment |
| LCI | Life cycle inventory |
| LCIA | Life cycle impact assessment |
| LSV | Linear sweep voltammetry |
| MA | Mass activity |
| MOR | Methanol oxidation reaction |
| MW | Microwave |
| MWAL | Microwave-assisted leaching |
| NPs | Nanoparticles |
| NPV | Net present value |
| OD | Ozone depletion |
| OPEX | Operational expenditure |
| ORP | Oxidation–reduction potential |
| ORR | Oxygen reduction reaction |
| PMF | Particulate matter formation |
| POF | Photochemical ozone formation |
| PGMs | Platinum-group metals |
| ROI | Return on investment |
| rpm | Revolutions per minute |
| RHE | Reversible hydrogen electrode |
| SEM | Scanning electron microscopy |
| SA | Specific activity |
| SAC | spent automotive catalyst |
| STEM | Scanning transmission electron microscopy |
| TEA | Techno-economic assessment |
| TRL | Technology readiness level |
| TEM | Transmission electron microscopy |
| WF | Water footprint |
| WACC | Weighted average cost of capital |
| XRD | X-ray diffraction |

## Data availability

The data supporting this article are included in the supplementary information (SI). Supplementary information: extended methods, GDEx thermodynamic reactions and equations, supplementary MWAL and GDEx characterisation data, electrocatalytic testing data, LCA inventory details, and TEA assumptions, calculations and sensitivity analyses. See DOI: https://doi.org/10.1039/d6su00190d.

## Acknowledgements

This research was funded by the European Union's Horizon 2020 research and innovation programme, under grant agreement no. 958302 (PEACOC). Views and opinions expressed are however those of the author(s) only and do not necessarily reflect those of the European Union or the European Health and Digital Executive Agency. Neither the European Union nor the granting authority can be held responsible for them. Omar Martínez Mora thanks SECIHTI-Mexico (former CONACYT-Mexico) for the doctoral scholarship no. 766618. All authors thank Kristof Tirez, Wilfried Brusten, Filip Beutels, and Karlien Duyssens for their dedication to the analytical measurements conducted in this paper. We thank Myrjam Mertens for her support with the XRD measurements, Diane van Houtven for her continued and meticulous technical support to the GDEx process, and Wendy Wouters for her unwavering commitment to MWAL experiments. The authors acknowledge Johnson Matthey collaborators for their valuable input, which supported the techno-economic assessment calculations of this work.

## References

1 European Commission, Press corner | European Commission: Statement 25/1552, 2025, https://ec.europa.eu/commission/presscorner/detail/en/statement_25_1552, accessed October 1, 2025.
2 A. E. Hughes, N. Haque, S. A. Northey and S. Giddey, Platinum group metals: A review of resources, production and usage with a focus on catalysts, *Resources*, 2021, **10**, 93.
3 European Commission: Directorate-General for Internal Market Entrepreneurship and SMEs I, M. Grohol, C. Veeh, *Study on the Critical Raw Materials for the EU 2023 – Final Report*, Publications Office of the European Union, 2023, doi/DOI: 10.2873/725585.
4 U.S. Geological Survey, About the 2025 Draft List of Critical Minerals, 2025, https://www.usgs.gov/programs/mineral-resources-program/science/about-2025-draft-list-critical-mineralsAC-2025/09/01, accessed October 1, 2025.
5 Department for Business and Trade, Department for Business Energy & Industrial Strategy. Resilience for the Future: The UK's Critical Minerals Strategy. London, UK, 2022, https://www.gov.uk/government/publications/uk-critical-mineral-strategy, accessed October 1, 2025.
6 Government of Canada, Critical minerals: an opportunity for Canada, 2025, https://www.canada.ca/en/campaign/critical-minerals-in-canada/critical-minerals-an-opportunity-for-canada.html, accessed October 1, 2025.
7 Australian Government; Critical Minerals Office, Australia's Critical Minerals List and Strategic Materials List 2024, https://www.industry.gov.au/publications/australias-critical-

minerals-list-and-strategic-materials-list, accessed October 1, 2025.
8 Ministry of Economy Trade and Industry (Japan), Metal Resources & Strategic Minerals | METI, 2025, https://www.meti.go.jp/policy/economy/economic_security/metal/index.html, accessed October 1, 2025.
9 International Energy Agency (IEA), Critical Mineral List in Korea 2023, https://www.iea.org/policies/17943-critical-mineral-list-in-korea, accessed October 1, 2025.
10 Ministry of Mines, Government of India, Critical Minerals for India. New Delhi, India, 2023, https://mines.gov.in/admin/download/649d4212cceb01688027666.pdf, accessed October 1, 2025.
11 H. Tang, Z. Peng, R. Tian, L. Ye, J. Zhang, M. Rao, *et al.*, Platinum-group metals: Demand, supply, applications and their recycling from spent automotive catalysts, *J. Environ. Chem. Eng.*, 2023, **11**, 110237, DOI: 10.1016/j.jece.2023.110237.
12 J. Matthey, *PGM Market Report May 2025*, Johnson Matthey Plc, 2025.
13 G. Nicol, E. Goosey, D. Ş. Yıldız, E. Loving, V. T. Nguyen, S. Riaño, *et al.*, Platinum Group Metals Recovery Using Secondary Raw Materials (PLATIRUS): Project Overview with a Focus on Processing Spent Autocatalyst, *Johns Matthey Technol Rev. JohnsTechnol Rev.*, 2021, **65**, 127–147, DOI: 10.1595/205651321X16057842276133.
14 R. Panda, M. K. Jha, D. D. Pathak. *Commercial Processes for the Extraction of Platinum Group Metals (PGMs). Rare Metal Technology 2018*, Springer; 2018, p. 119–130.
15 C. Saguru, S. Ndlovu and D. Moropeng, A review of recent studies into hydrometallurgical methods for recovering PGMs from used catalytic converters, *Hydrometallurgy*, 2018, **182**, 44–56, DOI: 10.1016/j.hydromet.2018.10.012.
16 T. J. Appleton, R. I. Colder, S. W. Kingman, I. S. Lowndes and A. G. Read, Microwave technology for energy-efficient processing of waste, *Appl. Energy*, 2005, **81**, 85–113, DOI: 10.1016/j.apenergy.2004.07.002.
17 S. W. Kingman, K. Jackson, S. M. Bradshaw, N. A. Rowson and R. Greenwood, An investigation into the influence of microwave treatment on mineral ore comminution, *Powder Technol.*, 2004, **146**, 176–184, DOI: 10.1016/j.powtec.2004.08.006.
18 Z. Peng, Z. Li, X. Lin, H. Tang, L. Ye, Y. Ma, *et al.*, Pyrometallurgical Recovery of Platinum Group Metals from Spent Catalysts, *JOM*, 2017, **69**, 1553–1562, DOI: 10.1007/s11837-017-2450-3.
19 C. A. Pickles, Microwaves in extractive metallurgy: Part 2–A review of applications, *Miner. Eng.*, 2009, **22**, 1112–1118, DOI: 10.1016/j.mineng.2009.02.014.
20 T. Abo Atia, W. Wouters, G. Monforte and J. Spooren, Microwave chloride leaching of valuable elements from spent automotive catalysts: Understanding the role of hydrogen peroxide, *Resour. Conserv. Recycl.*, 2021, **166**, 105349, DOI: 10.1016/j.resconrec.2020.105349.
21 T. Abo Atia and J. Spooren, Fast microwave leaching of platinum, rhodium and cerium from spent non-milled autocatalyst monolith, *Chem. Eng. Process. Process Intensif.*, 2021, **164**, 108378, DOI: 10.1016/j.cep.2021.108378.
22 T. Suoranta, O. Zugazua, M. Niemelä and P. Perämäki, Recovery of palladium, platinum, rhodium and ruthenium from catalyst materials using microwave-assisted leaching and cloud point extraction, *Hydrometallurgy*, 2015, **154**, 56–62, DOI: 10.1016/j.hydromet.2015.03.014.
23 F. Kukurugya, W. Wouters and J. Spooren, Microwave-assisted chloride leaching for efficient recovery of platinum group metals from spent automotive catalysts: An approach for chemical reagent reduction, *Clean Eng. Technol.*, 2025, **24**, 100868, DOI: 10.1016/j.clet.2024.100868.
24 R. A. Prato, V. Van Vught, S. Eggermont, G. Pozo, P. Marin, J. Fransaer, *et al.*, Gas Diffusion Electrodes on the Electrosynthesis of Controllable Iron Oxide Nanoparticles, *Sci. Rep.*, 2019, **9**, 15370, DOI: 10.1038/s41598-019-51185-x.
25 M. R. A. Prato, V. Van Vught, K. Chayambuka, G. Pozo, S. Eggermont, J. Fransaer, *et al.*, Synthesis of material libraries using gas diffusion electrodes, *J. Mater. Chem. A*, 2020, **8**, 11674–11686, DOI: 10.1039/D0TA00633E.
26 O. Martinez-Mora, G. Pozo, L. F. Leon-Fernandez, J. Fransaer and X. Dominguez-Benetton, Synthesis of platinum group metal nanoparticles assisted by CO2 reduction and H2 cogeneration at gas-diffusion electrodes, *RSC Sustain.*, 2023, **1**, 454–458, DOI: 10.1039/D3SU00046J.
27 O. Martinez-Mora, L. F. Leon-Fernandez, M. Velimirovic, F. Vanhaecke, K. Tirez, J. Fransaer, *et al.*, Platinum nanoclusters made by gas-diffusion electrocrystallization (GDEx) as electrocatalysts for methanol oxidation, *Adv. Mater.*, 2023, **4**, 6183–6191, DOI: 10.1039/D3MA00209H.
28 O. Martinez-Mora, K. Tirez, F. Beutels, W. Brusten, L. F. Leon-Fernandez, J. Fransaer, *et al.*, Exploring Pt-Pd alloy nanoparticle cluster formation through conventional sizing techniques and single-particle inductively coupled plasma—Sector field mass spectrometry, *Nanomaterials*, 2023, **13**, 2610, DOI: 10.3390/nano13182610.
29 L. F. Leon-Fernandez, A. Caballero-Ortiz, O. Martinez-Mora, J. Fransaer and X. Dominguez-Benetton, Mechanism and kinetics of gold recovery and Au nanoparticle synthesis by Gas-Diffusion Electrocrystallization (GDEx), *Electrochim. Acta*, 2023, **460**, 142592, DOI: 10.1016/j.electacta.2023.142592.
30 H. Ooka, M. C. Figueiredo and M. T. M. Koper, Competition between Hydrogen Evolution and Carbon Dioxide Reduction on Copper Electrodes in Mildly Acidic Media, *Langmuir*, 2017, **33**, 9307–9313, DOI: 10.1021/acs.langmuir.7b00696.
31 M. L. Grilli, A. E. Slobozeanu, C. Larosa, D. Paneva, I. Yakoumis and Z. Cherkezova-Zheleva, Platinum group metals: Green recovery from spent auto-catalysts and reuse in new catalysts—A review, *Crystals*, 2023, **13**, 550, DOI: 10.3390/cryst13040550.
32 S. Sui, X. Wang, X. Zhou, Y. Su, S. Riffat and C. Liu, A comprehensive review of Pt electrocatalysts for the oxygen reduction reaction: Nanostructure, activity, mechanism and carbon support in PEM fuel cells, *J. Mater. Chem. A*, 2017, **5**, 1808–1825, DOI: 10.1039/C6TA08580F.

33 X. Zhao, M. Yin, L. Ma, L. Liang, C. Liu, J. Liao, *et al.*, Recent advances in catalysts for direct methanol fuel cells, *Energy Environ. Sci.*, 2011, **4**, 2736–2753, DOI: 10.1039/C1EE01307F.
34 Y. Alvarez-Gallego, X. Dominguez-Benetton, D. Pant, L. Diels, K. Vanbroekhoven, I. Genné, *et al.*, Development of gas diffusion electrodes for cogeneration of chemicals and electricity, *Electrochim. Acta*, 2012, **82**, 415–426, DOI: 10.1016/j.electacta.2012.06.096.
35 International Organization for Standardization, *ISO 14044:2006 Environmental Management — Life Cycle Assessment — Requirements and Guidelines*, International Organization for Standardization, 2006.
36 M.-D. Bermúdez, F. J. Carrión, G. Martínez-Nicolás and R. López, Erosion–corrosion of stainless steels, titanium, tantalum and zirconium, *Wear*, 2005, **258**, 693–700, DOI: 10.1016/j.wear.2004.09.023.
37 K. Deng, Y. Xu, C. Li, Z. Wang, H. Xue, X. Li, *et al.*, PtPdRh Mesoporous Nanospheres: An Efficient Catalyst for Methanol Electro-Oxidation, *Langmuir*, 2019, **35**, 413–419, DOI: 10.1021/acs.langmuir.8b03656.
38 C. Liu, T. Wu, F. Zeng, X. Pan, G. Li, K. Teng, *et al.*, High-selective and effective carbon nanotubes supported ultrasmall PtPdRh electrocatalysts for ethanol oxidation, *Electrochim. Acta*, 2023, **437**, 141531, DOI: 10.1016/j.electacta.2022.141531.
39 M. V. Martínez-Huerta, N. Tsiouvaras, M. A. Peña, J. L. G. Fierro, J. L. Rodríguez and E. Pastor, Electrochemical activation of nanostructured carbon-supported PtRuMo electrocatalyst for methanol oxidation, *Electrochim. Acta*, 2010, **55**, 7634–7642, DOI: 10.1016/j.electacta.2009.09.082.
40 K. Tao, J. Wang, Y. Li, D. Xia, H. Shan, H. Xu, *et al.*, Short peptide-directed synthesis of one-dimensional platinum nanostructures with controllable morphologies, *Sci. Rep.*, 2013, **3**, 2565, DOI: 10.1038/srep02565.
41 M. Ł. Górzny, A. S. Walton and S. D. Evans, Synthesis of High-Surface-Area Platinum Nanotubes Using a Viral Template, *Adv. Funct. Mater.*, 2010, **20**, 1295–1300, DOI: 10.1002/adfm.200902196.
42 Y. Jiang, Y. Guo, Y. Zhou, S. Deng, L. Hou, Y. Niu, *et al.*, Synergism of Multicomponent Catalysis: One-Dimensional Pt-Rh-Pd Nanochain Catalysts for Efficient Methanol Oxidation, *ACS Omega*, 2020, **5**, 14805–14813, DOI: 10.1021/acsomega.0c01859.
43 Johnson Matthey. PGM management. Johnson Matthey, 2025, https://matthey.com/products-and-markets/pgms-and-circularity/pgm-management, accessed July 1, 2025.
44 Ecotrade Group, Ecotrade Group | Sell your scrap catalytic converters, 2025, https://www.ecotradegroup.com/en/, accessed June 25, 2025.
45 Eurostat, Electricity price statistics – statistics explained | Eurostat 2025, https://ec.europa.eu/eurostat/statistics-explained/index.php?title=Electricity_price_statisticsStatisticsExplainedElectricitypricestatistics, accessed October 12, 2025.
46 European Commission, European Critical Raw Materials Act, European Commission, 2025. https://commission.europa.eu/strategy-and-policy/priorities-2019-2024/european-green-deal/green-deal-industrial-plan/european-critical-raw-materials-act_en, accessed October 12, 2025.
47 European Commission, End-of-life vehicles regulation | Environment — European Commission 2025, https://environment.ec.europa.eu/topics/waste-and-recycling/end-life-vehicles_en, accessed October 8, 2025.
48 European Commission, Waste shipments | Environment — European Commission, 2025, https://environment.ec.europa.eu/topics/waste-and-recycling/waste-shipments_en, accessed October 12, 2025.